Depletion of atmospheric methane by iron induced activation of chloride

Sergej Bleicher, Julian Wittmer and Cornelius Zetzsch

Atmospheric Chemistry Research Laboratory, University of Bayreuth, Dr.-Hans-Frisch-Str. 1-3,

95448 Bayreuth, Germany

Abstract

Investigations on NaCl saltpans in an environmental simulation chamber under artificial sunlight show high concentrations of chlorine atoms in the gas phase if $FeCl_3$ is added to the salt mixture. The impact of chlorine atoms led in a direct experiment to a methane reduction of 8% within 24 h. This corresponds to a methane lifetime of only 12 days in a constantly illuminated chamber (or a half-life of 8 days). In quantitative measurements almost 10 million of Cl atoms per cm^3 were observed as peak concentrations in the chamber above mixtures of NaCl and 0.5% $FeCl_3$. This would decrease the lifetime of methane under atmospheric conditions of usually 8-10 years down to a hundredth of it. Typical values ranged from 10^5 to 10^6 Cl atoms per cm^3. The direct Cl measurements allowed us to calculate the Cl_2 source strength to reach a maximum of 8×10^{11} Cl_2 molecules per cm^3 and s within the first hour of tha experiment, corresponding to a Cl_2 mixing ratio of 30 ppbv at standard pressure.
The salt samples consisted of 100 g total mass with various mixing ratios of NaCl and $FeCl_3$, NaBr, catechol, oxalate, sulfate and $MgCl_2$. The additions of catechol, Na-oxalate and Na-sulfate led to a distinct reduction of the chloride activation by a complexation of the iron ions. Samples with added NaBr showed very high concentrations of Br atoms above 10^{10} atoms per cm^3, though only low Cl values.
Whether the activation of chloride still occurs under addition of other iron species like Fe_2O_3 remained unresolved. Pending questions are moreover a possible formation of organochlorine compounds and the absolute surface of the saltpan samples.

1 Introduction

There are many indications for an easier chloride activation in halide media in the presence of iron(III). Sunlight may photolytically reduce iron(III) halides to iron(II) and oxidize chloride at the same time. The oxidized chloride may afterwards be released to the gas phase by forming Cl_2 molecules (Gehlen, 1804, Eder, 1880, Lim, et al., 2008, Vione et al., 2006, Chiron et al., 2007, Khanra et al., 2008, Vione et al., 2005, Nadtochenko and Kiwi, 1998a, Nadtochenko and Kiwi, 1998b, Nadtochenko and Kiwi, 1998c, Machulek et al., 2006, Oeste, 2004). Chlorine atoms have more than a magnitude faster reaction rate constants towards methane in comparison to hydroxyl radicals at room temperature ($k_{CH4,Cl}$ = 1,1 10^{-13} $cm^3 molecules^{-1} s^{-1}$ (Bryukov et al., 2002), $k_{CH4,OH}$ = 6,7 10^{-15} cm^3 $molecules^{-1} s^{-1}$ (Srinivasan et al., 2005)). They initiate the degradation of methane to CO_2 by forming methyl radicals and HCl. Such activations of chloride may happen where iron and halide media come into contact under the influence of sunlight. Iron-containing salts appear relatively often in the natural environment:

- Mineral aerosol, which is blown from arid continental regions, comes into contact with sea salt aerosol above oceans (Trochkine et al., 2003; Tobo et al., 2010)
- Fly ash aerosol from volcanic eruptions as condensation nuclei for hydrogen chloride and sulfurous volcanic gases and water (Duggen et al., 2007; Langmann et al., 2010)
- Coastal regions, wetted by sea spray

- Intertidal zones, which may undergo particularly high iron mobilization by a step gradient of the reduction potential and faunal activity (Batel et al., 2003)
- Brine containing soils (Kotte and Schöler, 2010)
- Sediments covered with salt crusts, where biologically induced redox zoning can mobilize iron. This may lead to an enrichment of the salts or brines with iron.
- Coastal regions of the Arctic, where mineral and sea salt aerosol are sedimenting on concentrated brines (Spolaor et al., 2013a; Spolaor et al., 2013b); Spolaor et al., 2012 reported the contents of soluble iron in ice drilling cores; using this data one may conclude on the current iron input by sedimentation of mineral dusts.
- Examples of possible anthropogenic induced activation of chloride are salts on salt mine dumps or brine production facilties. Both salt sources contain between 20 mg/kg and 300 mg/kg of iron (Binenga, 2006; ur Rahman et al., 2010; Titler and Curry, 2011).
- Other possible examples of anthropogenic activation of chloride are open graduation works, where mineral brines are evaporated in contact with iron containing ground waters (Kirnbauer, 2008).
- One further source of iron in the marine boundary layer is the combustion of ship fuel. Soot aerosol containing iron oxides may form iron halides if it comes into contact with sea spray (Ito, 2013). It is known that sea spray may coagulate with other aerosols (Trochkine et al., 2003) to form mixed iron-seasalt aerosol nuclei. The amount of soluble iron emitted by ship traffic in the northern Atlantic and Pacific has been predicted for the year 2100 from model calculations to possibly contribute 30% to 60% to the total soluble iron in the atmosphere of those regions (Ito, 2013).

The deposition of mineral dust to sea water leads to algal bloom by iron fertilization. The algae again contribute to the binding of CO_2 from the atmosphere (Duggen et al., 2007). Moreover, the effect of iron on the methane depletion by activating chloride to chlorine should be at least on the same scale as other contributions to the depletion of greenhouse gases (Oeste and Ries, 2011). This is also indicated by the anti-correlation of CO_2 and methane to dust concentrations in time profiles derived from Antarctic and Greenlandic ice drill cores. Whenever the past atmosphere had high concentrations of dust – these reached to a factor of 50 of the present value – CO_2 and methane were in their minima and cold periods occurred. During the warm periods the concentrations of CO_2 and methane were in their maxima, while the air was almost free from dust (van der Pluijm and Sefcik, 2007). Recent studies by Levine et al. (2011, 2012) find hints at a depletion of methane by chlorine during the glacial periods. The iron containing loess dust, which occurred during the glacials, could be in context with such elevated, methane depleting chlorine mixing ratios. Further indicators for this hypothesis are the evidence for chlorine atoms in the diluted eruption cloud of the Eyjafjallajökull volcano (Baker et al., 2011) and the concentration minima of methane during the big volcano eruptions of the Earth's history (Gauci et al., 2008). The high-bitumen heavy oil ship fuel contains oil soluble transition metal compounds, particularly iron compounds (Madu et al. 2011). The combustion of those fuels generates Fe_2O_3 aerosols, which are rapidly converted to iron halides in the marine boundary layer. The already mentioned emission of soluble iron compounds caused by the increasing worldwide ship traffic might reach 30-60% of the natural sources in the northern hemisphere by 2010 (Ito 2013).

The sponsors of this study believe that at least some issues of natural greenhouse depletion by iron(III) photolysis mentioned above can be technically optimized, so that these can be applied to force a climate cooling economically and without danger to the environment and neither to the human health. In particular under consideration are tropospheric aerosols in the marine boundary layer with enriched iron concentrations to force the methane and CO_2 depletion. The production and the activity of such aerosols have been described by Oeste and Ries (2011) under the name "ISA-Verfahren" (ISA-technique). The depletion of CO_2 occurs in the first place in analogy to the environmental processes by deposition of the iron aerosol to the sea and fertilization of algae (Duggen et al., 2007, Langmann et al., 2010, Lindenthal et al., 2012). Two types of aerosols are considered: (I.) Fe_2O_3 aerosol and (II.) iron-(III)-chloride aerosol. While the second is already an iron

halide aerosol, the first undergoes ageing in the marine boundary layer under the influence of SO_2, NO_X, O_2, water vapor and sea spray to an iron halide aerosol. In a further case the "ISA-technique" describes (III.) an aerosol, in which chloride-containing nuclei are covered with an iron compound surface, which again is able to release chlorine. In contrast to (I.) and (II.) the technique described in (III.) is meant to be used for methane depletion only. All techniques have patents or patents are pending (Oeste, 2010, Meyer-Oeste, 2003, 2012).

1.2 The aim of this investigation

The objective of this study is the investigation of chlorine emission by photolysis of iron(III) complexes and an assessment of methane depletion. In positive outcomes, the release of halogens and the depletion of methane should be quantified. The experiments are carried out on NaCl saltpan samples under tropospheric-like conditions using artificial sunlight in a Teflon chamber (Buxmann et al., 2012). The main experimental parameter is the content of iron(III) in the salt samples. Also the influence of oxalate (or oxalic acid), catechol, bromide, sulfate and $MgCl_2$ on the activation of halides and the depletion of methane shall be regarded, since these compounds are often found in natural salts and aerosols. In the case of observation of a halogen activation by iron(III) and a subsequent methane depletion by chlorine, further investigations are desired, where the efficiency of the ISA method on aerosols should be quantified.

2. Instrumental set-up and methods

2.1 Parameters of investigation

The selection of the investigated parameters refers to the (I.) and (II.) versions of the ISA process and to the chlorine emitting layer, which are described by (III.) ISA version. This takes into account that the original high iron content in the aerosol or in the emitting layer is diluted below the 1% mark by various processes, such as photoreduction (Zuang et al, 1992), coagulation with organic aerosols (Trochkine et al., 2003) or with the water of tropospheric clouds (Deguillaume et al., 2010) or uptake of gaseous species (in particular HCl) by the ocean surface (Zhang and Isakawa , 2001 Tobo et al., 2010, Shi et al., 2011, Johnson and Meshkidze, 2011, Fu et al., 2012). The following text describes and gives reasons why and which compounds, in addition to NaCl and iron(III) chloride, should be assayed for their influence on the release of chlorine. Of particular interest are organic compounds as they occur in the organic aerosol in the troposphere, such as oxalic acid and its salts (Myriofalitakis et al., 2011). Dicarboxylic acids alter the light absorption of iron species by complex formation (Zhu et al., 1993, Weller and Herrmann, 2009). Oxalic acid has the highest complexation potential here, as very long known (Eder, 1880). It is also known that catechol is actively used by microbes in natural aerosols (Claeys et al., 2012), in the vegetated compartments of water, in soil sediment and in biofilms (Borges et al. , 2005 Merce et al., 2005) as a reversible redox mediator to reduce species such as iron for external breathing (Lovely et al., 1996, Coates et al., 1997). Molecular oxygen reacts under formation of 1,2-quinone with the functional groups of catechol to form H_2O_2 (Miura et al., 1998, Kim et al., 2011). H_2O_2 in turn oxidizes iron (II), remaining from the photo Fenton reaction, to iron (III) and forms hydroxyl radicals. The latter are supposed to release chlorine from the liquid phase (Krause et al., 2011). It is therefore assumed that the ubiquitous catechols may trigger the photo Fenton reaction. While the main tropospheric sources of H_2O_2 are OH and HO_2 radicals (eg. Stewart, 2004), its essential precursors in the limnic, humic milieu are catechols in humic-like substances (Southworth and Voelker, 2003). Recent studies indicate that the humic H_2O_2 sources are also important for the atmosphere (Herrmann et al., 2007, Moonshine et al., 2008a, 2008b). Bromide is one of the ubiquitous substances in natural salts. Bromide salts are well soluble and hygroscopic, as like as alkali-sulfates and some alkaline earth metal salts. Under Arctic conditions the freezing of sea water leads to salt brines on the ice surface, where hygroscopic iron (III) salts could also be enriched. Frost flowers in such brines can multiply the active surface and accelerate the transition chemistry (e.g. Herrmann et al., 2007). This transition chemistry in not bound to frost flowers only, but can also occur in clouds. The high concentrations of trace compounds in the brine, which are increased by extrusion of crystallization process, also accelerate the chemistry including the Fenton reaction (Arakaki et al., 2004 Grannas et al., 2007). An activation of the dissolution of iron oxides by feezing process in the presence of sunlight has been detected (Kim et al., 2010). However, brine processes and their consequences should not be the subject of this preliminary investigation, but remain a subject of the subsequent more detailed study. This study focuses only on some of the common hygroscopic salts contained in seawater. Bromide is a far easier oxidizable compound compared to chloride (e.g. Barcellos da Rosa et al., 2003). Thus even small amounts of bromide have a high impact on the chloride chemistry. Hypobromous acid may recombine with chloride and form bromine monochloride, which is released to the gase phase quickly and is photolyzed to Br and Cl by sunlight. This way bromide acts as a catalyst for the activation of chloride. Therefore it is necessary to proof the impact of bromide on the iron induced chlorine activation.

The natural activation of halogens has been found over a wide range of temperatures and relative humidities: as like in the Polar spring, where the “bromine explosion” (e.g. Pöhler et al., 2010) occurs at temperatures significantly below the freezing point and high relative humidities (which is also indicated by growing frost flowers). Low temperatures below the freezing point were also measured during the halogen activation in the Eyjafjallajokull eruption plume at altitudes of 3-6 km over Ireland and the Arctic Ocean (Baker et al., 2011). The activation of bromide was also observed in other eruption plumes (von Glasow et al., 2009, Bobrowski et al., 2009). “Chlorine explosions” were already observed in our laboratory (Bleicher 2012, Siekmann, 2010) at room temperature. The

halogen activation in the western Australian salt lakes is a subject of investigation by the DFG research group 763 “Natural Halogenation Processes in the Environment” (HALOPROC), where gaseous halogen species were found at temperatures near 40 °C and low relative humidity (Krause, 2013). Qualitative studies on the catalytic activation of halogens by iron(III) suggest an efficient reaction between 20 to 30 °C, relatively independent of humidity of the iron(III) layer (Oeste, 2004). The effect of the relative humidity and temperature on the catalytic halogen activation by iron(III) will also remain as subject of the subsequent, detailed analysis. For the present investigation a relative humidity of >50% and a temperature of 20 °C were chosen for all experiments. Those are typical annual average values on the surface if the Australian salt lakes, which are examined in the HALOPROC project (Buxmann et al., 2012). The influence of rising relative humidity at night due to the falling temperatures and in particular its influence on the phase change of the hygroscopic salt layers were not considered yet. The examination of those influences remains also as an object to further research, while the present study will focus on the variation of the salt sample composition. A number of 12 salt samples were measured under almost similar conditions, according to the recipes given below:

1. NaCl 100%
2. NaCl 95%, $MgCl_2$ 5%
3. NaCl 99.5%,NaBr 0.5%
4. NaCl 98%, Na-oxalate 2%
5. NaCl 98%, Catechol 2%
6. NaCl 98%, $FeCl_3$ 2%
7. NaCl 93%, Na_2SO_4 5%, $FeCl_3$ 2%
8. NaCl 97.5%, NaBr 0.5%, $FeCl_3$ 2%
9. NaCl 96%, Na-Oxalate 2%, $FeCl_3$ 2%
10. NaCl 96%, Catechol 2%, $FeCl_3$ 2%
11. NaCl 96%, $FeCl_3$ 2%, oxalic acid 2%
12. NaCl 91%, Na_2SO_4 5%, $FeCl_3$ 2%, oxalic acid 2%

The salt layer was prepared by evaporating a brine, wherein the solid salts were completely dissolved abd the dried again. The evaporation residue was mostly crushed and spread on a Teflon holder inside the chamber. The sample was then exposed to the filtered light of the solar simulator. To demonstrate the photolytic reduction of the iron (III) to iron (II) a part of the illuminated sample was shaded from the light emitter, as described in 2.3. The shaded part reacts with a suitable reagent by forming a color other than the illuminated part. The quantitative measurements of the chlorine atom formation were accomplished by monitoring the decay of a previously injected mixture of selected hydrocarbons (HC), including an inert standard. The HC monitoring was performed by gas chromatography with a time resolution of 15 min, as described in section 2.3. The amount of Cl atoms and OH radicals was calculated from the characteristic HC decay (Zetzsch and Behnke, 1992).

2.2 Experimental set-up

The chamber is made of Teflon film(FEP200A, DuPont). The film is fixed on three aluminum rings of 1.33 m diameter to form a cylinder of 2.8 m height and is suspended above a solar simulator. Inside the chamber is a transparent Teflon film holder for exposing the salt samples (Figure 1). The light

emission of the solar simulator is comparable to the tropospheric sun light on the 50th latitude in the tropospheric summer (Figure 2).

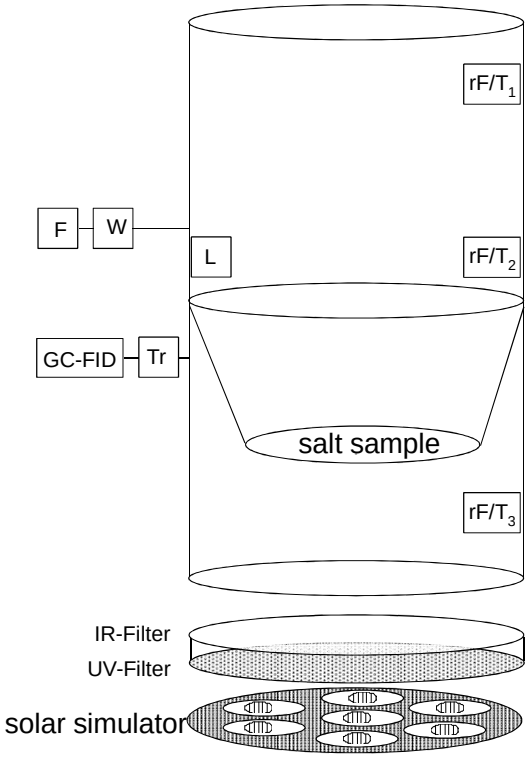

Figure 1: Simulation chamber above the solar simulator. The components are a flow controller (F), a humidifier (W), a fan (L), a gas chromatograph with flame ionization detector (GC-FID), air dryers (Tr) and combined sensors for relative humidity (RH) and temperature (T),

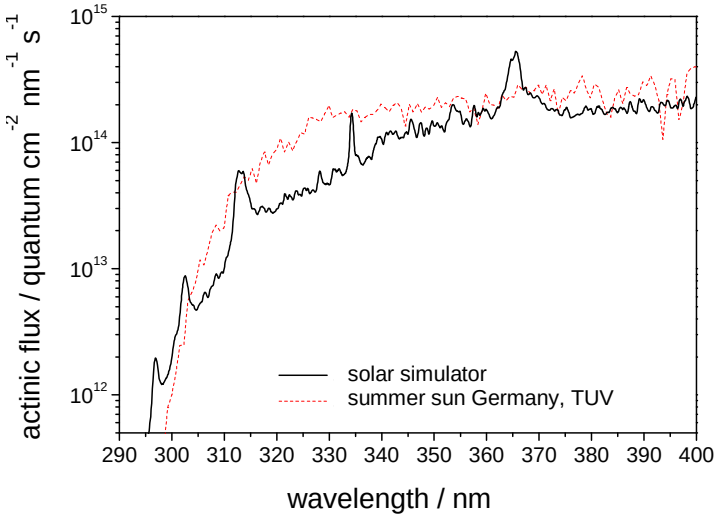

Figure 2: The spectrum of the solar simulator in comparison to a calculation of the radiative transfer model TUV (Madronich and Velders, 1999) for 50° latitude in summer (Bleicher, 2012)

2.3 A quantitative method for measurement of Cl and Br atoms and OH radicals

The direct evidence of the methane depletion is complicated due to its long life time. Even when the lifetime is decreased to a fraction due to high Cl concentrations, a direct experiment has to be prepared to run for many days. However, since the rate constants of the reaction of chlorine atoms and OH radicals with methane are precisely known, the proof of chlorine atom formation is sufficient. Their evidence is provided here by a degradation pattern of a particular hydrocarbon mixture (Zetzsch and Behnke, 1992). An additional indicator could be an accelerated ozone depletion, which can be precisely measured by a chemiluminescence analyzer (UPK, 8002). The evidence that the chlorine is activated by the photolysis of iron(III) chloride to iron(II) will be given by spraying potassium ferricyanide on irradiated salt. Only the exposed surfaces react to the Prussian blue charge transfer pigments due to the occurrence of iron(II) (Adhikamsetty and Jonnalagada, 2009).

The simultaneous measurement of OH, Cl and Br radicals is achieved by an indirect but quantitative method, which can be used under the nearly tropospheric like conditions of the simulation chamber. The radicals are not observed directly but their reaction partners, which are a set of certain hydrocarbons (HC). These HCs, namely 2,2-dimethylpropane (DMP), 2,2-dimethylbutane (DMB), 2,2,4-trimethylpentane (TMP), toluene, and the inert standard perfluorohexane (PFH), have different rate constants of their reactions with OH, Cl, and Br (see Table 1). The HCs are added to the chamber air before the experiment. The measurement of their time profiles allows solving/integrating the corresponding differential equation:

$$-d[HC_i]_t/dt = k_{i,OH}, [HC_i]_t[OH]_t+k_{i,Cl}[HC_i]_t[Cl]_t+k_{i,Br}[HC_i]_t[Br]_t$$

$$\text{resp.} \quad -d \ln[HC_i]_t/dt = k_{i,OH}[OH]_t+k_{i,Cl}[Cl]_t+k_{i,Br}[Br]_t$$

for all reactive HC_i and experimental times *t*. Since the system has three unknowns [OH], [Cl], and [Br], but four reactive hydrocarbon species, it is over-determined. This can be used to calculate a statistical error between the single results. In the absence of Br atoms, the statistical analysis improves accordingly. The detection limit of this method is directly related the rate constants from Table 1 and the sensitivity of the gas chromatography system. The detection limit can be given to 10^4 cm^{-3} for Cl atoms, 10^6 molecules cm^{-3} for OH radicals and about 10^9 atoms cm^{-3} for Br. The HC are be measured by a gas chromatograph (GC) with a flame ionization detector (FID). The gas chromatograph (Siemens Sichromat-2) is equipped with a fully automated enrichment equipment (custom build), and achieved a HC detection limit of about 50 ppt (for 20 area units). It is connected with a 8 m long 1/16 "stainless steel capillary with the chamber, which is heated to 50 ° C and is continuously flushed with a flow rate of 0.1 l/min with chamber air. A gas dryer (Nafion, DuPont, custom build) between the stainless steel capillary and the chamber lowers the air humidity to a dew point of -20 °C. A GC measurement takes 14 minutes, including the HC enrichment of 6 minutes (fig. 3). Each peak area is integrated afterwards and is correlated to the HC_i mixing ratio in the chamber. All single measurements taken together give a time profile of an individual HC. Analytical functions are fitted to the HC time profiles, which gives an interpolation and averaging between the measurements. Depending on the experimental results either (bi-) exponential or sigmoidal functions are used for fitting the data points. The HC mixing ratio has to be constant in darkness, since the halogen activation is a photolytic reaction. Therefore, the dark mixing ratios are used as a zero point (*t*=0) for fitting. The HC peak areas in the chromatogram are linearly related to the mixing ratio, therefore an instrument calibration is actually not necessary.

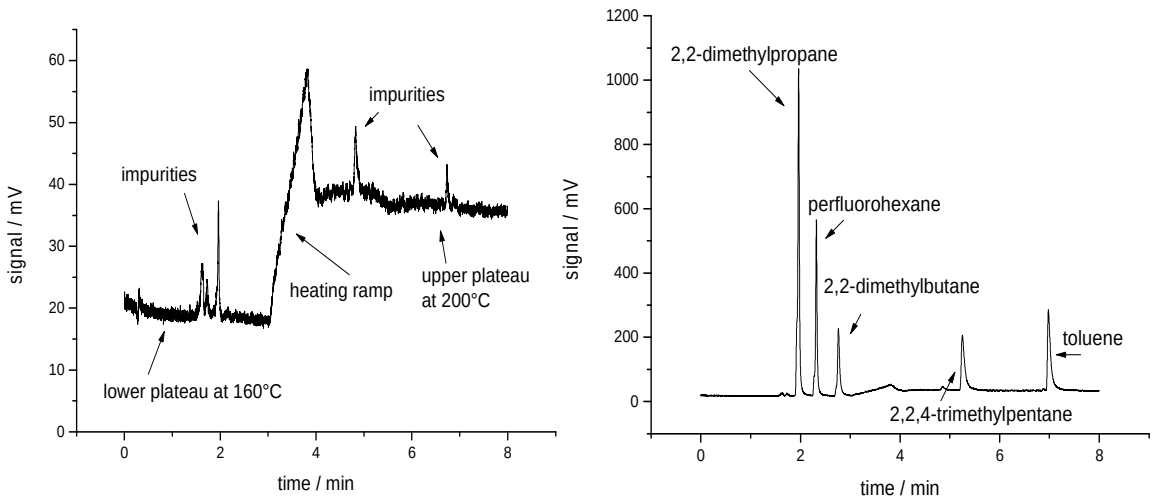

Figure 3: Gas chromatography measurement of zero-air (left) and a measurement with injected hydrocarbons (right). The GC oven temperature is set to 160 °C at the beginning to separate the peaks of DMP, PFH DMB then the oven is heated to 200 °C for the rapid detection of TMP and toluene.

Table 1: Rate constants (in cm^3 $molecule^{-1}$ s^{-1}) of the observed hydrocarbons with the radicals at 298 K. Perfluorohexane is completely inert to OH, Cl and Br at room temperature.

Hydrocarbon	k_{OH} [1]	k_{Cl} [2]	k_{Br} [3]
Methane	6.7e-15	1.1e-13	
2,2-Dimethylpropane (DMP)	8.25E-13	1.1e-10	
2,2-Dimethylbutane (DMB)	2.23E-12	1.68E-10	
2,2,4-Trimethylpentane (TMP)	3.34E-12	2.31E-10	6.79E-15
Toluene	6.16E-12	5.9E-11	1.3E-14
Perfluorhexane	-	-	-

2.4 Preparation of the salt pan

The salts were weighted to a total mass of 100 g and afterwards dissolved in 500 ml of bi-distilled water. The solution was dried on a Teflon sheet in a crystallizing bowl in an oven at 45 ° C for 48 h. The oven was purged with zero air (dew point -70 °C) during the drying. Afterwards the dry salt sample was either ground in a mortar or placed directly into the simulation chamber. An overview of the sample pre-treating is shown in Table 20v. The chamber was flushed with humid zero air for 24 h afterwards.

[1] Atkinson 2003
[2] Atkinson and Aschmann 1985
[3] Barnes et al, 1989

3 Results

3.1a. Zero experiment on NaCl (NaCl_A)

A NaCl sample of 100 g mass (p.a. Aldrich) was placed onto the sample holder in the simulation chmaber and humidified for 24 h by humid air. An initial relative humidity of 52% at 20 °C was achieved. A chromatogram of the zero air in before the injection of HC to the chamber is shown in Figure 3 (left). The mixture of hydrocarbons, which was injected to the chamber, consisted of:

- 120 µl 2.2 dimethylpropan (18.8 ppb DMP)
- 0.2 µl perfluorohexane (6.9 ppb; inert standard, PFH)
- 0.1 µl 2,2-dimethylbutane (5.3 ppb, DMB)
- 0.1 µl 2,2,4-trimethylpentane (4.3 ppb, TMP)
- 0.1 µl toluene (6.6 ppb)

A chromatogram of the chamber air in the dark with hydrocarbons injected is shown in Figure 3 (right). Four of such chromatograms in the dark were measured with a time gap of 12.5 minutes and checked for similarity. Afterwards the solar simulator was switched on shuttered to avoid the intensity increase of the lamps by their heat up of three minutes. The shutter was opened and the chamber was suddenly exposed to light. The initial NO_X (NO_X = NO + NO_2) mixing ratio was 3-4 ppb, these values could already trigger an activation of chloride (Bleicher et. al, 2013, in preparation, Buxmann, 2012). The dilution corrected measurement data is shown in Figure 4 (left). While toluene shows a significant decrease, the alkanes have been only slightly reduced, which is an indication of low chlorine atoms concentration. The concentrations of OH and Cl radicals (Figure 4, right) were derived from the functions fitted (shown in Table 2) to the measurement data. The concentration of OH radicals has the typical value of about 5 × 10^6 cm^{-3}. Chlorine atoms had a concentration of ~5 × 10^4 cm^{-3}, which is slightly above the detection limit.

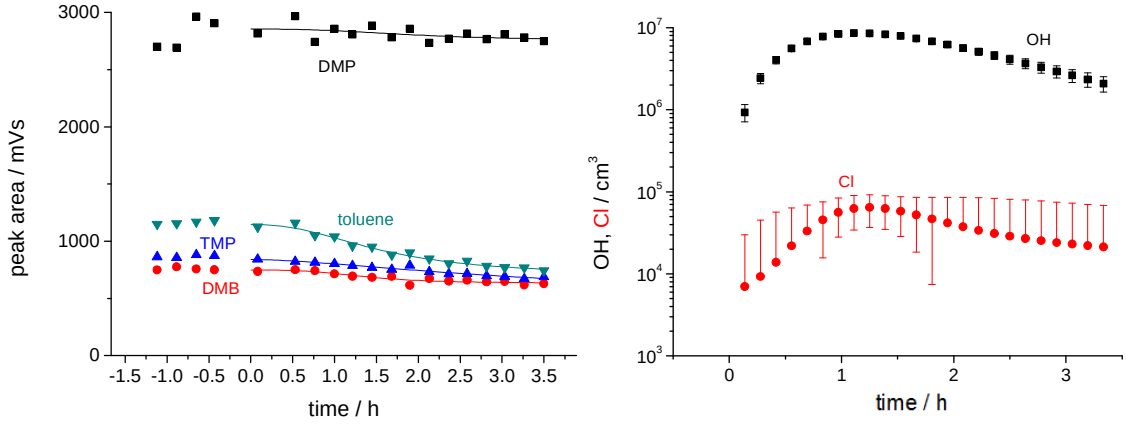

Figure 4: Shown are the HC measurements over a salt sample of 100g of NaCl (left) and the calculated concentrations of OH and Cl radicals (right). The depletion maximum was reached after 75 minutes of illumination.

An increase of the ozone mixing ratio to 10 ppb was observed during the illumination due to mechanism R1 (see chapter 4). The maximum of the ozone mixing ratio is correlated with the maximum of OH and Cl.

Table 2: Fitting functions on the measurement data from Figure 4 to derive the concentrations of OH und Cl

Hydrocarbon	Fitting function /mVs
2,2-Dimethylpropane (DMP)	$2753 + \frac{2855 - 2753}{1 + (\frac{t}{7070s})^{2.73}}$
2,2-Dimethylbutane (DMB)	$633 + \frac{747 - 633}{1 + (\frac{t}{4942s})^{3.46}}$
2,2,4-Trimethylpentane (TMP)	$505 + \frac{842 - 505}{1 + (\frac{t}{12730s})^{1.59}}$
Toluene	$698 + \frac{1147 - 698}{1 + (\frac{t}{5600s})^{2.36}}$

3.1b. Zero experiment on NaCl with ozone and NO_X (NaCl_B)

The salt sample from experiment 3.1.a was exposed to illumination a second time. In addition high mixing ratios of Ozone (240 ppb) and NO_X (130 ppb) were injected to the chamber air. Comparable HC mixing ratios were injected to the chamber. During the period of six hours illumination a weak reduction of alkanes was observed (Figure 5, left). The analytical OH, Cl evaluation (compare Table 3) derives slightly increased concentrations of OH and Cl (Figure 5, right), which is reasoned by ozone and NO_2.

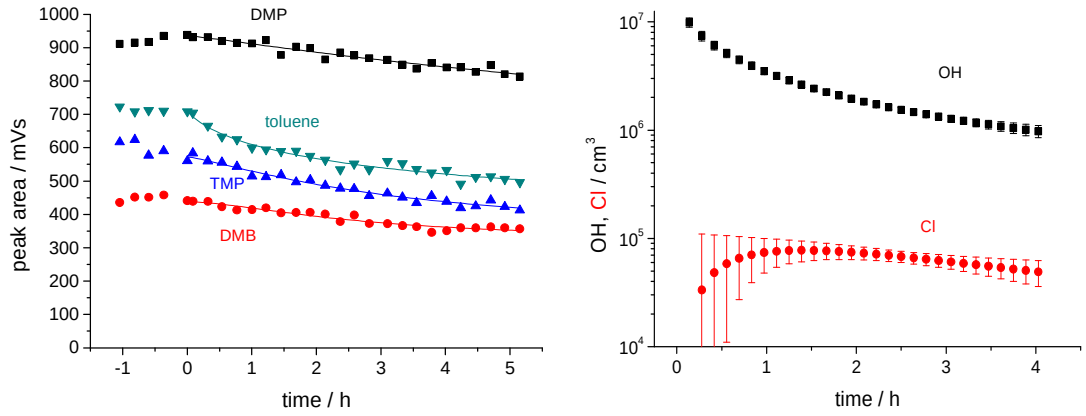

Figure 5: Repeating measurement with initial 240 ppb of ozone and 130 ppb of NO2 added. The radical concentration is increased

Table 3: Fitted functions to the HC measurement data from Figure 5 (left)

Hydrocarbons	Fitting function /mVs
2,2-Dimethylpropane (DMP)	$552 + \frac{936 - 552}{1 + (\frac{t}{39164s})^{1.15}}$
2,2-Dimethylbutane (DMB)	$322 + \frac{437.6 - 322}{1 + (\frac{t}{9816s})^{1.66}}$
2,2,4-Trimethylpentane (TMP)	$323 + \frac{572 - 323}{1 + (\frac{t}{12560s})^{1.26}}$
Toluene	$358 + \frac{715 - 358}{1 + (\frac{t}{11515s})^{0.76}}$

3.2 Zero experiment on NaCl and $MgCl_2$ ($MgCl_2$_A)

The salt sample of 95 g NaCl and 5 g MgCl was completely dissolved in bi-distilled water and dried in an oven at 80 °C for 48h. The grinding of the salt was difficult due to the samples high hygroscopicity. The salt was put on the sample holder in the chamber and flushed overnight with humid zero air. On the following day, the HC were injected and the salt pan was exposed the light of the solar simulator, see Figure 6 (left). The greatest loss occurred to toluene, suggesting OH radical as the most important in this experiment. The analytical calculations of the OH and Cl concentrations are summarized in Figure 6 (right).

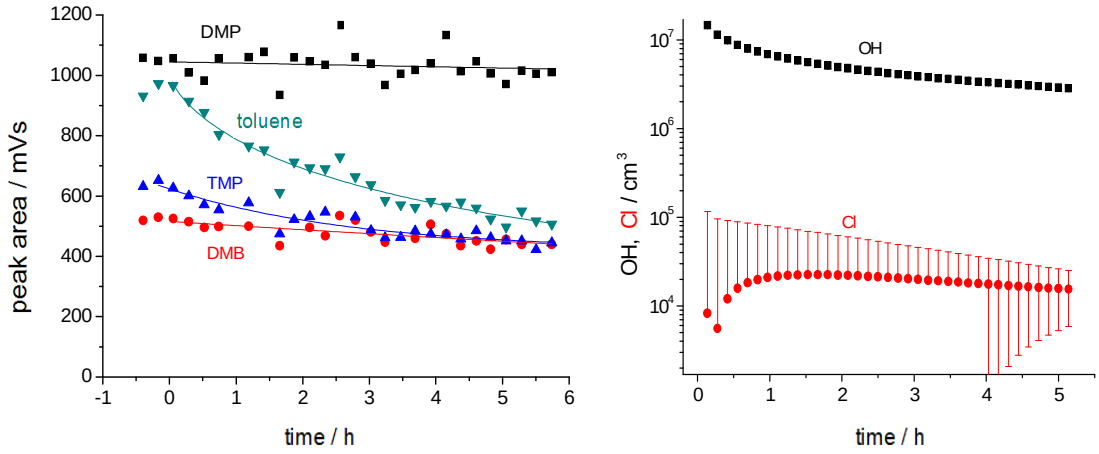

Figure 6: Measured HC decrease above a NaCl/$MgCl_2$ salt sample (left) and the derived radical concentrations (right). Despite the high hygroscopicity oft the sample the Cl concentration was not increased.

Table 4: Fitted functions to the measurement data of Figure 6 (left).

Hydrocarbon	Fitting functions/mVs
2,2-Dimethylpropane (DMP)	$1044e^{-t/910022s}$
2,2-Dimethylbutane (DMB)	$515e^{-t/132564s}$
2,2,4-Trimethylpentane (TMP)	$420 + 203e^{-t/10124s}$
Toluene	$\frac{1005}{1 + (\frac{t}{21461s})^{0.72}}$

3.3 Zero experiment on NaCl and NaBr (NaBr_A)

Systematic measurements on NaCl / NaBr salt samples have been previously published by Buxmann et al., 2012. The published measurements show a correlation between the activation of bromide and the relative humidity. It is known that even small portions of bromide can ease the activation of chloride due to mechanism R4 (see chapter 4).

The experiment was carried out on a 99.5 g NaCl, 0.5 g NaBr sample. A fast depletion of toluene and 2,2,4-trimethylpentane was observed during the illumination (Figure 7, left). Since both substances are known to react with bromine (Table 1), the concentration of bromine atoms was derived from their depletion (Figure 7, right). Also a significant activation of chloride could be observed here.

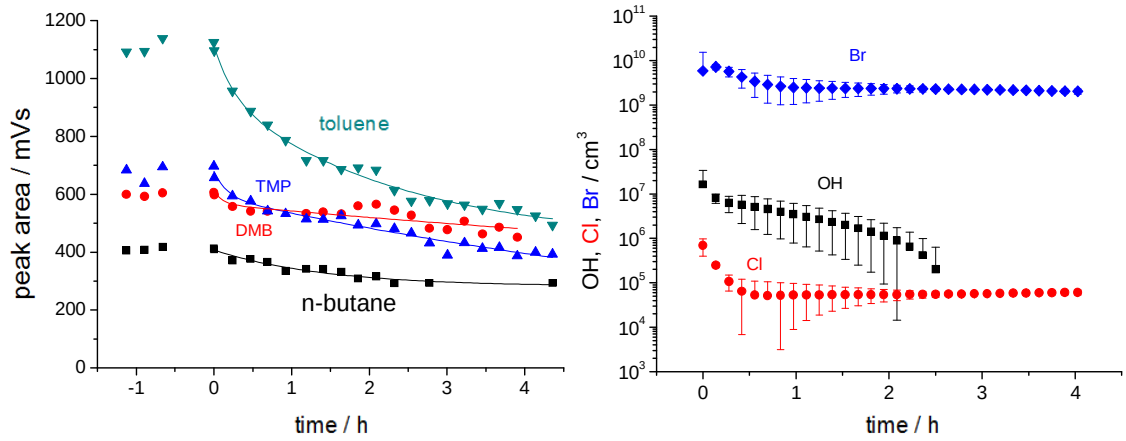

Figure 7: HC-curves over a NaCl / NaBr pan (left) and calculated radical data (right). A fast loss of TMP and toluene was observed, while the alkanes remained almost constant. This results in constantly high concentrations of Br atoms, also the concentration of Cl atoms is increased during the first hour.

Table 5: (bi)-exponential fitting functions to the data shown in Figure 7

Hydrocarbon	Fitting function /mVs
n-Butane	$281 + 126e^{-t/5173s}$
2,2-Dimethylbutane (DMB)	$254 + 301e^{-t/59566s} + 45e^{-t/386s}$
2,2,4-Trimethylpentane (TMP)	$44 + 67e^{-t/594s} + 550e^{-t/32140s}$
Toluene	$439 + 516e^{-t/8180s} + 157e^{-t/881s}$

3.4 Zero experiment on NaCl and Na-oxalate

The NaCl / Na-oxalate sample consisted of 98 g of NaCl, and 2 g of sodium oxalate. The salt was grinded after the recrystallization. The salt was placed on the sample holder in the chamber and was humidified overnight. A rel. humidity of 55% at 20 ° C was reached. Four chromatograms were measured in the dark after the injection of the HC mixture. The solar simulator was switched on and a strong , but delayed depletion of toluene was observed. The alkanes decreased slowly, but constantly (see Figure 8, left). For the analysis of the radical concentrations exponential functions were fitted to the alkane measurement data (Table 6). To fit the toluene data a sigmoidal function was used, resulting in a convex curvature of the OH concentration. Indicating an initially ozone free. The NOx/RO2-cycle generated ozone due to the injected HC and NOx. More important is the observed increase of Cl-atoms in this experiment.

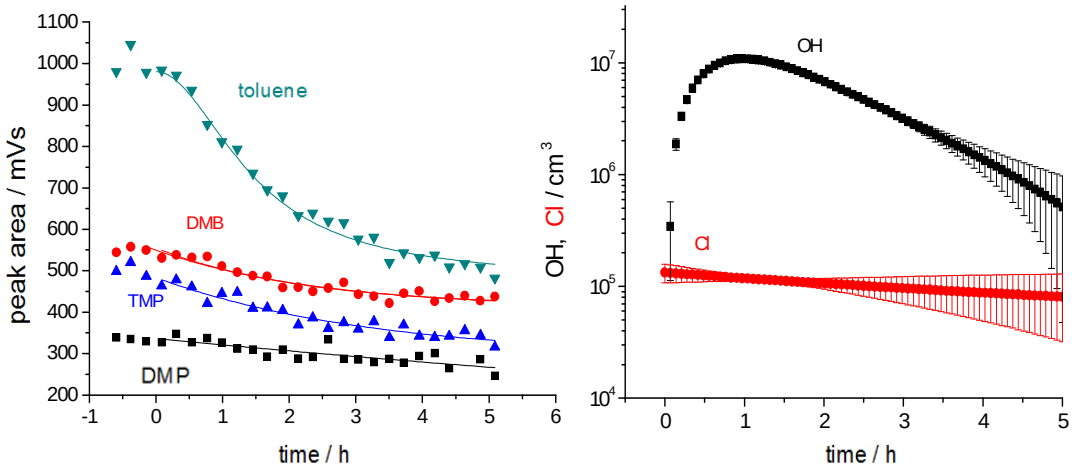

Figure 8: Course of the week on a NaCl / Na-oxalate salt pan (left) and calculated from the OH and Cl concentrations (right). The chlorine atoms are significantly above the detection limit.

Table 6: Fitted functions to the HC data points of Figure 8

Hydrocarbon	Fitting functions/mVs
2,2-Dimethylpropane (DMP)	$336e^{-t/78390s}$
2,2-Dimethylbutane (DMB)	$414 + 140e^{-t/7940s}$
2,2,4-Trimethylpentane (TMP)	$92 + 191e^{-t/11609s}$
oluene	$477 + \frac{981 - 477}{1 + (\frac{t}{5244s})^{1.98}}$

3.5 Zero experiment on NaCl and catechol

NaCl (98 g) and catechol (2 g) were dissolved in ca. 500 ml bi-distilled water. The solution was dried in an oven and the residuum was ground. The sample was put in the chamber and humidified for 24 h, than it was illuminated for two hours. The obtained data shows only a slightly reduction of the hydrocarbons (Figure 9, left). Analytical calculations of the radical concentrations are summarizes by (Figure 9, right). Both radical species, OH and Cl were close to the detection limit.

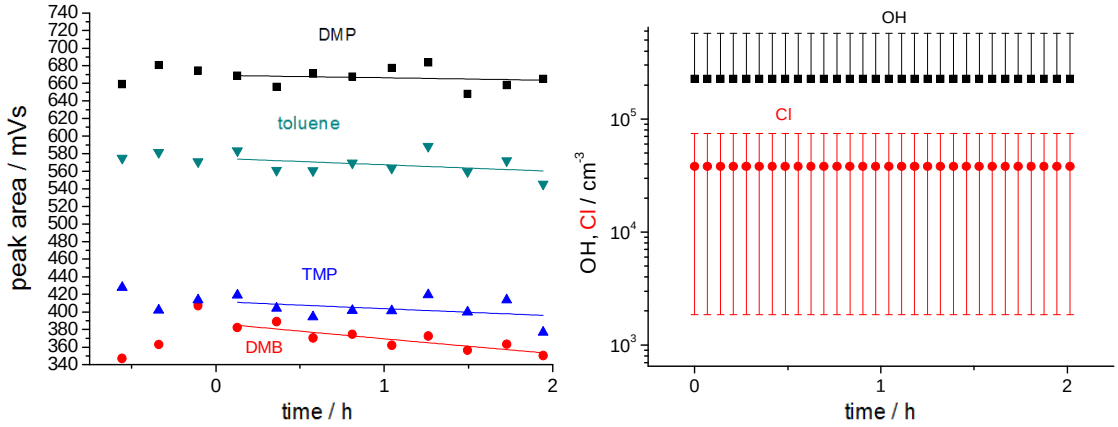

Figure 9: Slow HC depletion of KW over a NaCl and catechol salt mixture. Cl and OH were just above the detection limit.

Table 7: Fitting functions to the GC data shown in Figure 9 with long HC life times

Hydrocarbons	Fitted functions/mVs
2,2-Dimethylpropane (DMP)	$669e^{-t/688727s}$
2,2-Dimethylbutane (DMB)	$387e^{-t/77326s}$
2,2,4-Trimethylpentane (TMP)	$411e^{-t/179313s}$
Toluene	$574e^{-t/274227s}$

3.6 NaCl and iron chloride

After completing the zero experiments, samples with additional iron were prepared and measured. The first sample had 98 g NaCl and 2 g FeCl3. Both salts were dissolved in 500 ml of bi-distilled water in a glass bowl of 30 cm diameter for drying in an oven for 48 h at 40 °C. To speed up the drying, the oven was flushed with zero grade air. The dry sample was crushed with a mortar, were the hygroscopic salt got humid due to the ambient air. A further grinding was not possible under such conditions. The crushed, but sticky salt was placed on the sample holder in the chamber. A part of the salt was covered from both sides with aluminum foil (30 × 30 cm) to shade it. The chamber was closed and purged with humid zero air for 48 h, and a rel. humidity of 52% at 20 ° C was reached. Measurements 3.6a and 3.6b were carried out on this sample.

3.6a NaCl and $FeCl_3$

After the hydrocarbon were injected, their mixing ratios remained constant in the dark. The solar simulator was switched on and its shutter was opened after three minutes of preheating. This led to a rapid depletion of HC with a total loss within 30 minutes (Figure 10, left). Sigmoidal functions were used to fit and interpolate the data (see Table 8) to derive the radical concentrations in, right. Due to the extreme activation of chloride the temperature and humidity sensors of the chamber were irreparably damaged.

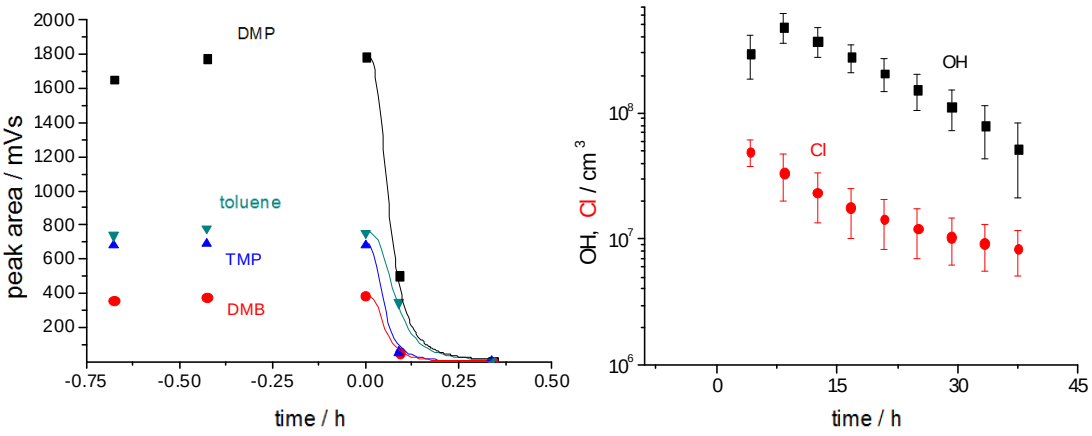

Figure 10: KW measurement on a FeCl3/NaCl salt pan with 2% FeCl3 addition and adapted to evaluate sigmoidal curves. The measurement at time zero was actually held at -10 minutes and was moved to a very rapid decrease of plausible interpretation of these few data points. In the last chromatogram peaks of toluene, TMP and DMB were no longer present, their values were arbitrarily set to 0.1.

Table 8: Sigmoidal functions represent the measurement data from, left

Hydrocarbon	Fitting functions/mVs
2,2-Dimethylpropane (DMP)	$\frac{1804}{1+(\frac{t}{226s})^3}$
2,2-Dimethylbutane (DMB)	$\frac{387}{1+(\frac{t}{188s})^3}$
2,2,4-Trimethylpentane (TMP)	$\frac{696}{1+(\frac{t}{173s})^3}$
Toluene	$1+\frac{758-1}{1+(\frac{t}{288s})^3}$

3.6b NaCl and $FeCl_3$

The measurement 3.6a was repeated 24 h later with higher HC mixing ratios to improve the radical calculation. The chamber was purged with humid zero air for preparation. Under day time conditions a fast HC depletion was observed in the first measurement hour (Figure 11, left). Their decay slowed down afterwards, probably due to the drying of the salt sample. The illumination of the salt pan lasted for more than five hours. The solar simulator was switched off and the chamber was opened and the aluminum foil removed. The shaded and the illuminated salt were sprayed with potassium hexacyanoferrate (III), which colored the illuminated salts blue, while the shaded part remained orange (see Figure 12). This indicates the photolytic reduction of iron-(III) to iron-(II).

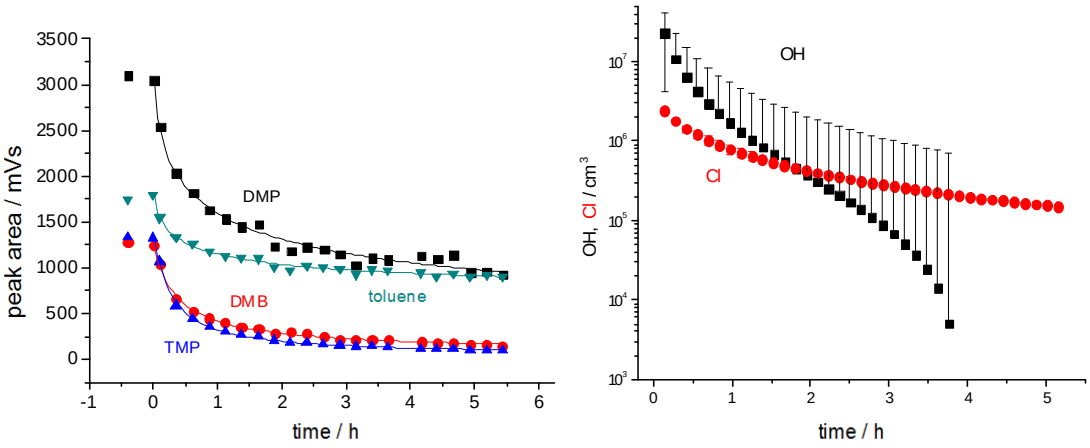

Figure 11: Depletion of HC in a repeat measurement above the salt sample from experiment 3.6a (left) and the derived OH und Cl concentrations (right)

Table 9: Fitted sigmoidal functions to the experimental HC data shown in Figure 11 (left) to derive the radical concentrations shown in the same figure (right)

Hydrocarbon	Fitting functions/mVs
2,2-Dimethylpropane (DMP)	$109 + \frac{3451 - 109}{1 + (\frac{t}{2309s})^{0.51}}$
2,2-Dimethylbutane (DMB)	$82 + \frac{1264 - 82}{1 + (\frac{t}{1381s})^{0.96}}$
2,2,4-Trimethylpentane (TMP)	$53 + \frac{1376 - 53}{1 + (\frac{t}{1376s})^{1.064}}$
Toluene	$625 + \frac{1997 - 625}{1 + (\frac{t}{1453s})^{0.53}}$

Figure 12: Salt sample from experiments 3.6a and 3.6b. The sample was partly shaded to show the photolytic reduction of iron (III) to iron (II) by spraying potassium hexacyanoferrate (III) on the sample, which forms Prussian blue pigments with iron-(II)

3.6c NaCl and $FeCl_3$

The previously planned experiment No. 11 with 20% $FeCl_3$ was modified to 0.5% $FeCl_3$ due to the high concentration of chlorine in the experiments 3.6a and 3.6b. Seven subsequent experiments were carried out on a newly prepared saltpan to prove the re-oxidation of Fe (II) to Fe (III) during night time. No treatment was done during night time.

In the first experiment 3.6c a fast depletion of the alkanes was measured during the first two hours, while a significant depletion of toluene occurred in the first hour only, Figure 13 (left). The measurement data can be reproduced well by sigmoidal functions (Table 10). The radical evaluation returns low OH values, but high Cl concentrations Figure 13 (right).

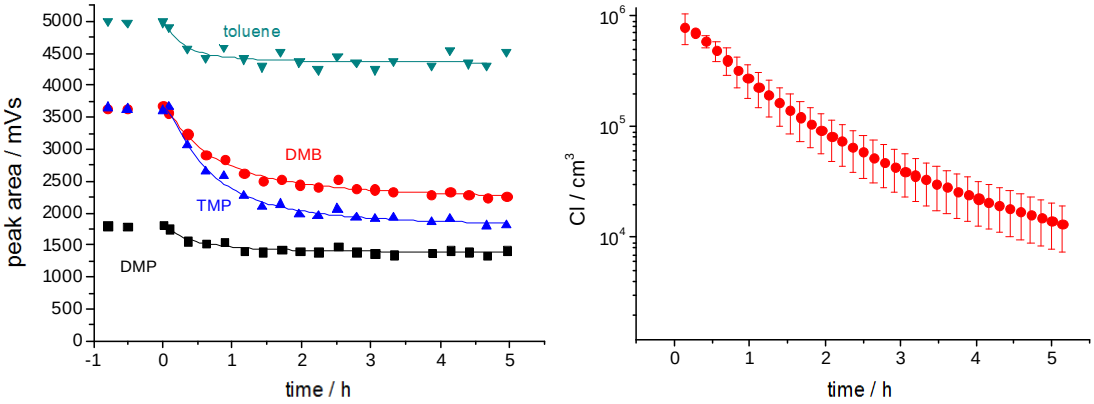

Figure 13: HC depletion above a NaCl/$FeCl_3$-sample (left) was caused by Cl-atoms (right). OH radicals were not observed.

Table 10: Sigmoidal functions represent the HC data shown in Figure 13

Hydrocarbon species	Fitting function/mVs
2,2-Dimethylpropane (DMP)	$1367 + \frac{1826 - 1367}{1 + (\frac{t}{1252s})^{1.18}}$
2,2-Dimethylbutane (DMB)	$2172 + \frac{3682 - 2172}{1 + (\frac{t}{2345s})^{1.28}}$
2,2,4-Trimethylpentane (TMP)	$1763 + \frac{3660 - 1763}{1 + (\frac{t}{2208s})^{1.52}}$
Toluene	$4344 + \frac{5001 - 4644}{1 + (\frac{t}{906s})^{1.356}}$

3.6d NaCl and FeCl3

The next experiment in the series was carried out on the following day. Although nearly the same amount of hydrocarbons was injected Figure 14 (left), the observed radical concentration was higher Figure 14 (right) than in the previous experiment 3.6c. A correlation with the humidity cannot be given since the the T/RH sensors have been damaged by HCl gas previously.

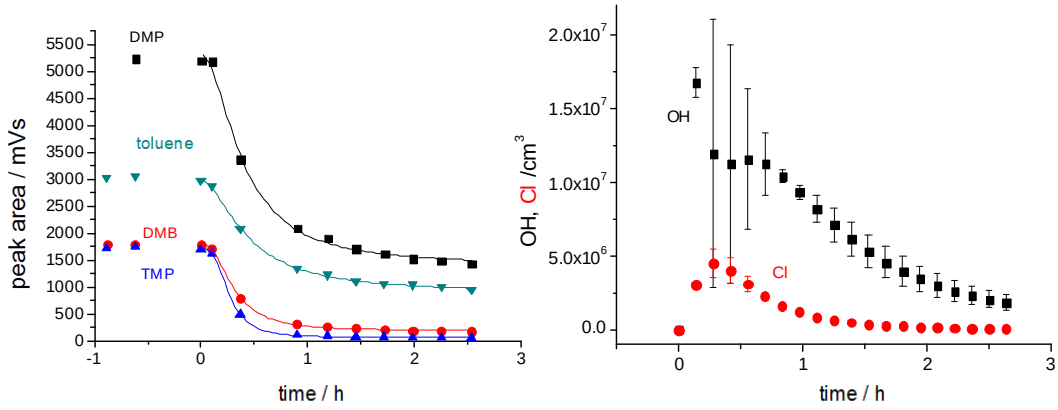

Figure 14: HC measurement data above the salt sample from experiment 3.6c. The radical evaluation with sigmoidal functions gives a maximum Cl maximum concentration of 5×10^6 atoms cm^{-3} after 20 minutes. High OH concentrations could be observed, In contrast to the previous experiment

Table 11: Fitted sigmoidal functions to the HC data from experiment 3.6d

Hydrocarbon species	Fitting functions/mVs
2,2-Dimethylpropane (DMP)	$1389 + \frac{5315 - 1389}{1 + (\frac{t}{1405s})^{1.9}}$
2,2-Dimethylbutane (DMB)	$2172 + \frac{3682 - 2172}{1 + (\frac{t}{2345s})^{1.28}}$
2,2,4-Trimethylpentane (TMP)	$1763 + \frac{3660 - 1763}{1 + (\frac{t}{2208s})^{1.52}}$
Toluene	$4344 + \frac{5001 - 4644}{1 + (\frac{t}{906s})^{1.36}}$

3.6e NaCl and $FeCl_3$

A repeating experiment on the sample 3.6c in a time distance of 24 h to 3.6d shows a fast HC depletion within the first hour (Figure 15, left). Although the depletion slows down for all HC, it remains significant; so that the entire concentration curve is well reproduced by bi-exponential functions (see Table 12). The achieved concentrations of OH and Cl were now slightly lower, see Figure 15 (right).

Table 12: fitted bi-exponential functions to represent the HC measurement data from experiment 3.6e.

Hydrocarbon species	Fitting function/mVs
2,2-Dimethylpropane (DMP)	$1633 + 226e^{-t/424s} + 1739e^{-t/104372s}$
2,2-Dimethylbutane (DMB)	$498 + 186e^{-t/1505s} + 1031e^{-t/42206s}$
2,2,4-Trimethylpentane (TMP)	$685 + 256e^{-t/815s} + 789e^{-t/19752s}$
Toluene	$1059 + 183e^{-t/386s} + 2014e^{-t/67378s}$

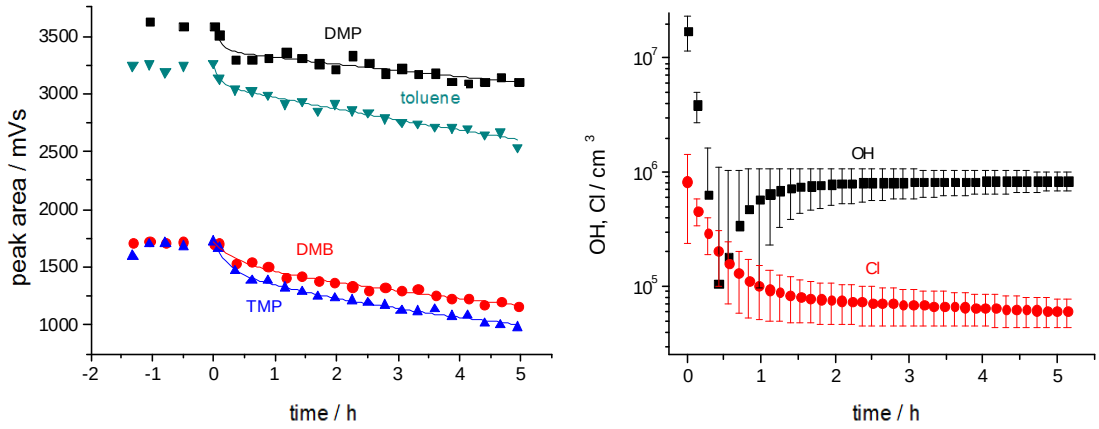

Figure 15: repeating measurement on the salt sample 3.6c. The evaluation of the HC data (left) gives almost constant radical concentrations after an hour (right).

3.6F NaCl and FeCl3

This experiment is not described here due to complications during the measurement. The air humidifier was turned off by a power cut, and the desired air humidity could not be reached. There were also difficulties with the enrichment equipment, so not HC could be measured. The analysis of the available data shows a concentration of chlorine atoms below 10^5 cm^{-3} and an OH concentration of less than 10^6 cm^{-3} at day conditions.

3.6g NaCl and FeCl3

The next experiment of the series was done 7 day later. The HC data shows a bi-exponential behavior, Figure 16 (left) and Table 13. Again, the high Cl atom concentrations fall rapidly to a stable plateau after 30 minutes, Figure 16 (right).

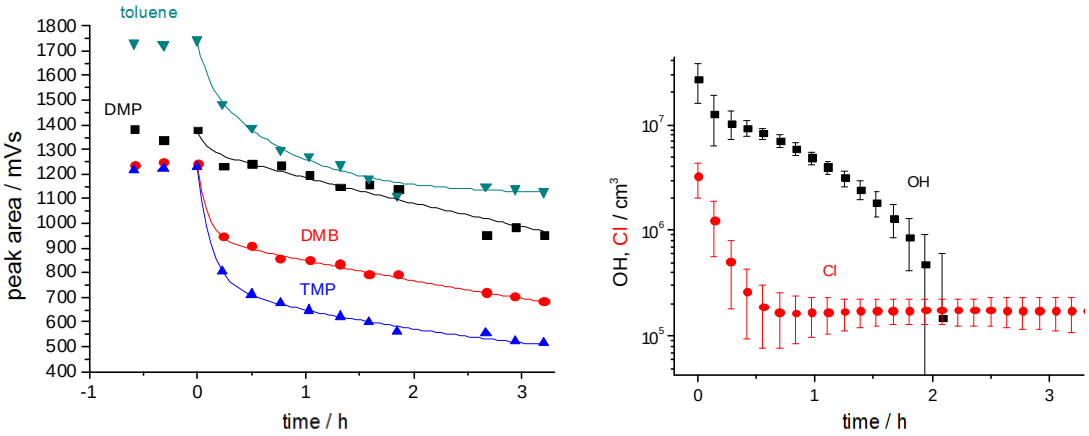

Figure 16: HC-data obtained above the salt sample 3.6c (left) and the evaluated radical concentrations (right)

Table 13: bi-exponential functions, which represent the measurement data oft he experiment 3.6g

Hydrocarbon species	Fitting function/mVs
2,2-Dimethylpropane (DMP)	$1300e^{-t/39338s} + 76e^{-t/300s}$
2,2-Dimethylbutane (DMB)	$303e^{-t/358s} + 940e^{-t/35897s}$
2,2,4-Trimethylpentane (TMP)	$381 + 376e^{-t/10632s} + 470e^{-t/467s}$
Toluene	$1116 + 142e^{-t/317s} + 484e^{-t/2967s}$

3.6h NaCl and $FeCl_3$

In this experiment it was planned to observe the methane depletion directly. However, it failed due to gas leaks in the methane analyzer.

3.6i NaCl and $FeCl_3$

A particle formation experiment was carried out on the salt sample 3.6c. The data shows a slightly higher particle concentrations above a saltpan compared to an empty, but new chamber, figure 17.

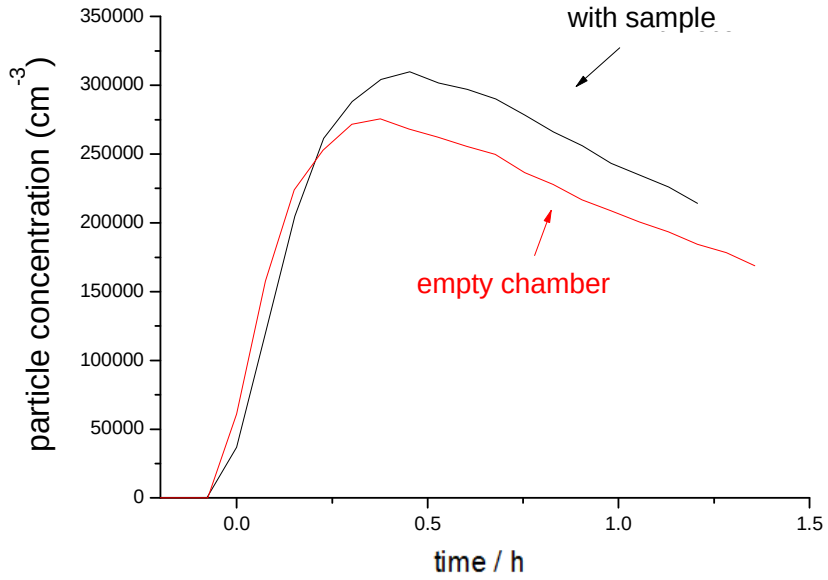

Figure 17: particle growing above a salt sample in comparison to an empty chamber

3.6j NaCl and $FeCl_3$

The last experiment of the series on the sample 3.6c had again no initial radical concentration peaks. Instead observed was a constant Cl plateau, Figure 18, derived from sigmoidal functions, Table 14.

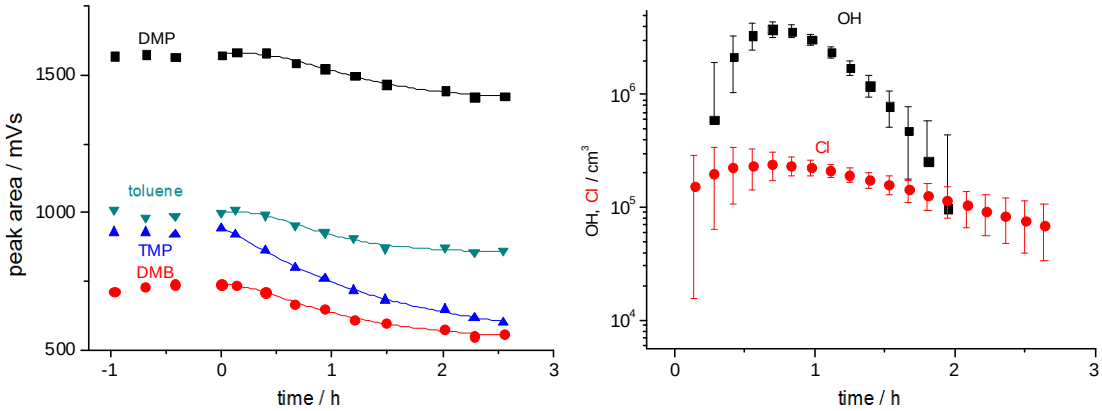

Figure 18: HC data measured in the run 3.6j (left) and the evaluated radical concentrations (right)

Table 14: Sigmoidal functions represent the HC data measured in run 3.6j

Hydrocarbon species	Fitting function/mVs
2,2-Dimethylpropane (DMP)	$1398 + \frac{1583 - 1398}{1 + (\frac{t}{4514s})^{2.66}}$
2,2-Dimethylbutane (DMB)	$515 + \frac{740 - 515}{1 + (\frac{t}{3866s})^{1.86}}$
2,2,4-Trimethylpentane (TMP)	$440 + \frac{943 - 440}{1 + (\frac{t}{5130s})^{1.265}}$
Toluene	$847 + \frac{1004 - 847}{1 + (\frac{t}{3340s})^{2.67}}$

3.6k. NaCl and FeCl3 - Direct observation of methane depletion

A new sample of 2 g of FeCl3 salt and 98 g of NaCl was prepared to observe the methane reduction directly. A hydrocarbon analyzer (Bendix Model 8202) was used to measure methane. 9 ppm of methane were injected into the chamber to be well above the detection limit of 200 ppb. The dilution flow was set to 4 l / min to keep over pressure in the chamber and prevent contamination. The measured results are shown in Figure 19.

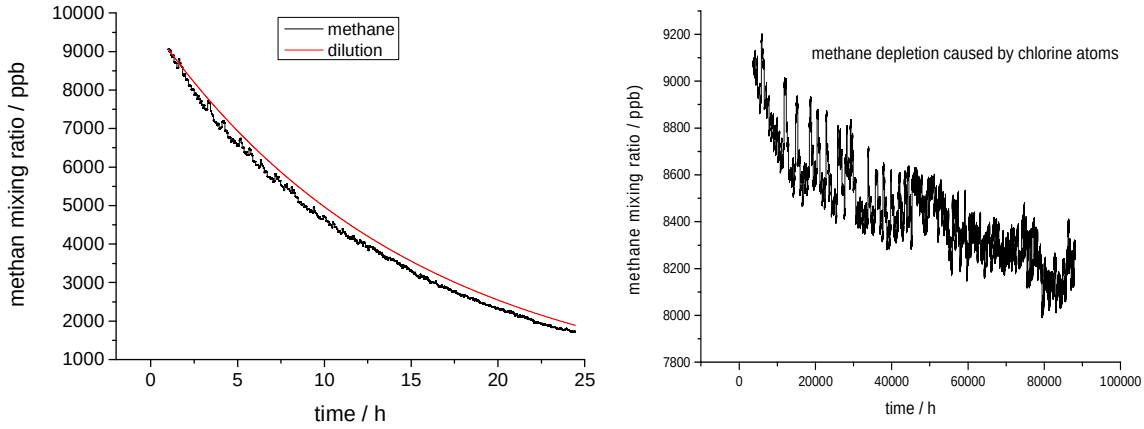

Figure 19: Direct observation of methane depletion by chlorine radicals. Raw measurement data and the dilution is shown on the left, while the dilution corrected methane depletion is shown on the right.

3.7 $FeCl_3$ and sodium sulphate

The mass mixing ratios of the salt for this experiment were 93 g NaCl, 5 g Na_2SO_4 and 2 g of $FeCl_3$. The salt was dissolved, recrystallized and afterwards milled with a ball mill. The salt sample became pale yellow color after recrystallization, in contrast to the upper experiments where the salts were bright orange. The fine grained and dry sample was placed in thin layers of the sample holder and exposed to light. A clear depletion of toluene, DMB and TMP was observed, while DMP remained virtually unchanged, Figure 20 (left) and Table 15. The activation of the chloride has been suppressed by the sulfate, as Figure 20 (right) shows.

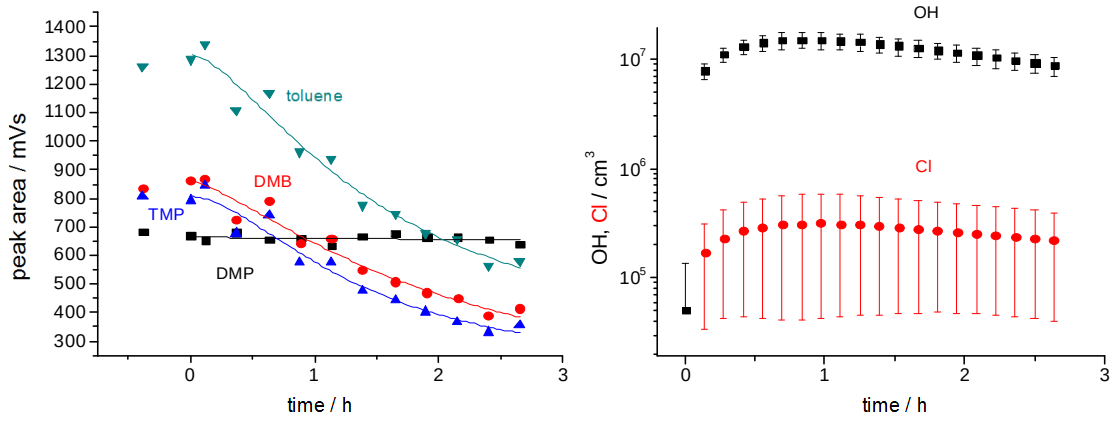

Figure 20: HC data above a Na_2SO_4/$FeCl_3$-sample (left) and calculated radical concentrations (right)

Table 15: Fitting functions represent the HC data from Figure 20 (left)

Hydrocarbon species	Anpassungsfunktion/mVs
2,2-Dimethylpropane (DMP)	$664.65e^{-t/577015}$
2,2-Dimethylbutane (DMB)	$42 + \frac{860 - 42}{1 + (\frac{t}{7534s})^{1.38}}$
2,2,4-Trimethylpentane (TMP)	$169 + \frac{808 - 169}{1 + (\frac{t}{5033s})^{1.72}}$
Toluene	$238 + \frac{1303 - 238}{1 + (\frac{t}{5555s})^{1.56}}$

3.8 $FeCl_3$ and sodium bromide

During the experiment on the NaBr/FeCl3/NaCl sample little depletion of DMP and DMB was observed, while TMP and toluene were greatly reduced (Figure 21, left). Both, toluene and TMP are known to react with Br atoms (see Table 1). Since their rate constants are slow the concentration of Br-atoms must have been extremely high. The radical evaluation shows over 10^{10} bromine atoms per cm3, with a slow exponential decay (Figure 21, right). Chlorine atoms and OH were also present, but not to the extent of the experiments 3.6. Such high Br concentrations were reproduced in two other experiments (not shown).

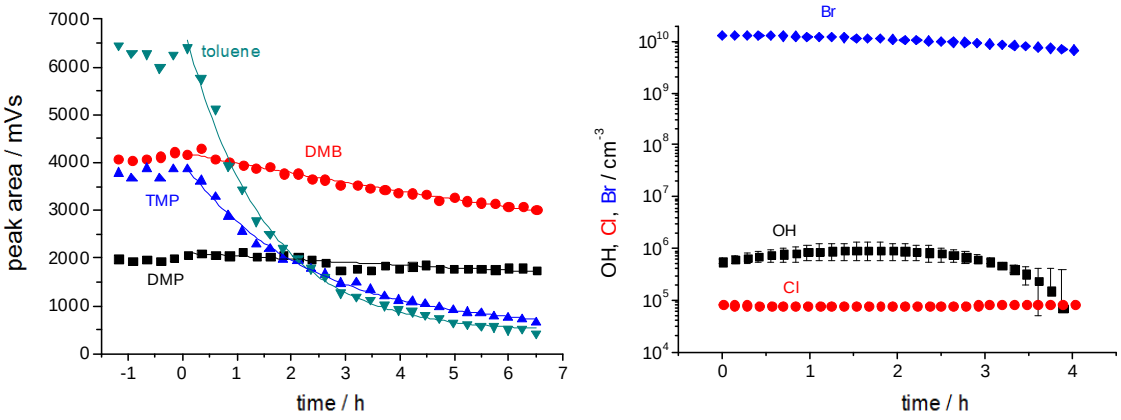

Figure 21: Depletion of toluene and trimethylpentane over a NaCl/FeCl3/NaBr sample (left) due to extremely high concentrations of Br atoms (right)

Table 16: Functions to represent the HC measurement data from experiment 3.8

Hydrocarbon species	Fitting function/mVs
2,2-Dimethylpropane (DMP)	$2108e^{-t/111000s}$
2,2-Dimethylbutane (DMB)	$4206e^{-t/68077s}$
2,2,4-Trimethylpentane (TMP)	$528 + \frac{6.6 \times 10^6 - 528}{1 + e^{\frac{t+61007}{8078s}}}$
Toluene	$60 + \frac{2.6 \times 10^6 - 450}{1 + e^{\frac{t+31238}{5213s}}}$

3.9 FeCl 3 and Na-oxalate

The salt components of this sample (96 g NaCl, 2 g of FeCl3 and 2 g Na-oxalate) were dissolved in bi-least-water and recrystallized in a drying oven. The dried salt pan was carefully lifted from the crystallizing dish and placed into the Teflon chamber. The liquid nitrogen, used to enrich the hydrocarbons for measuring depleted during the experiment after 30 minutes and had to be refilled. This led to a measurement stop for 75 minutes, between 0.5h - 1.5h (Figure 22,left). Nevertheless, the concentration profiles could be reproduced well, since they show little change over the 3.5h experimental time of light exposure (Table 17). Both, the release of Cl-, and of OH radicals were strongly suppressed in this experiment, their concentrations are just above the detection limit (Figure 22, right).

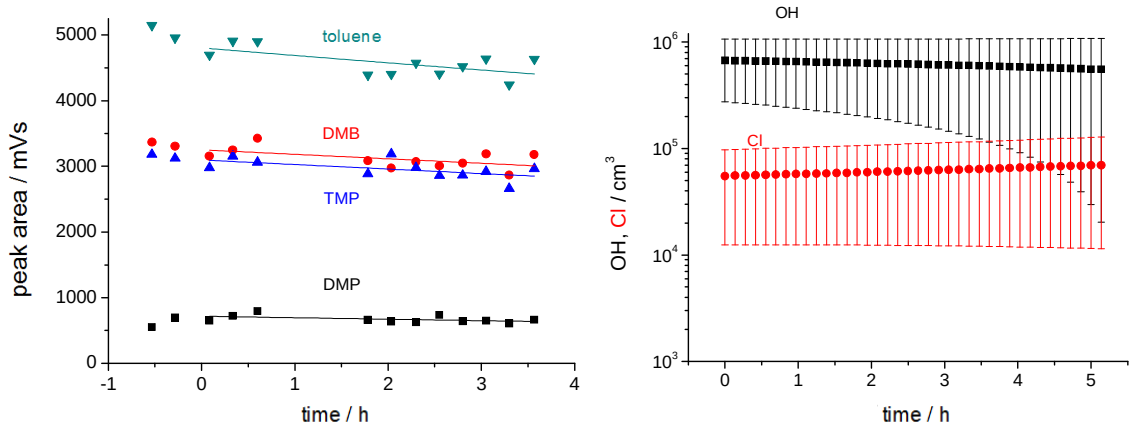

Figure 22: Measurement data above a Na-oxalate enriched salt sample (left) and the calculated radicals (right)

Table 17: Linear and exponential functions represent the HC data from Figure 22 (left)

Kohlenwasserstoff	Anpassungsfunktion/mVs
2,2-Dimethylpropan (DMP)	$754 - 0.01t/s$
2,2-Dimethylbutan (DMB)	3302–0.024t/s
2,2,4-Trimethylpentan (TMP)	$3161 - 0.026t/s$
Toluol	$4862e^{-t/12573s}$

3.10 Catechol and $FeCl_3$

The dissolved mixture of 96 g of NaCl and 2 g of $FeCl_3$ changed its color to black after addition of 2g catechol. After crystallization, the black salt pan was placed as one piece on the sample holder into the Teflon chamber. During the experiment almost no HC depletion was observed (Figure 23, left). The OH / Cl analysis here under 10 6 OH radicals and 5 × 103 atoms per cm3 of chlorine, see Figure 25 (right).

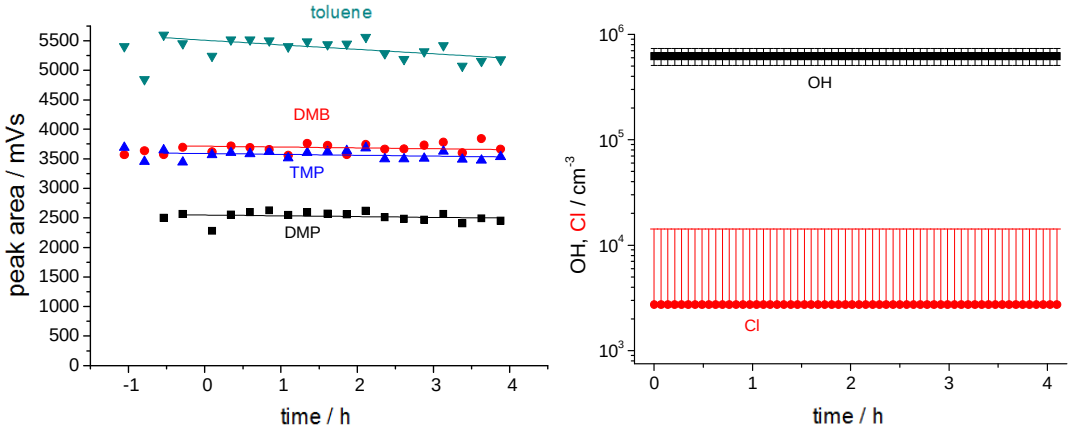

Figure 23: During the experiment with added catechol almost no change of HC concentrations was observed

3.11 $FeCl_3$ and oxalic acid

Previous measurement on $FeCl_3$ with an addition of Na-oxalate (3.9) showed an inhibition of iron induced chloride activation. A measurement with an addition of oxalic acid should clear out whether the mentioned inhibition is an effect of pH. A mixture of 96 g NaCl, 2 g of FeCl3 and 2 g oxalic acid was dissolved in 0.5l bi-distilled water and recrystallized. The crystallized salt was placed in one piece into the chamber on the sample holder. The experiment showed a depletion of alkanes mainly (Figure 24, left) and therefore a high chlorine concentration. The analytical evaluation of the radical concentrations indicates almost no presence of OH radicals (Figure 24, right and Figure 25, left). The fact than almost no OH radicals were present can be proofed by plotting the normalized concentrations of each HC species versus the normalized concentration of TMP (Figure 25, right). The slopes give a ratio of the rate constants of Table 1. For DMB/TMB, the ratio of Cl rate constants is 0.73 (0.76 in the experiment), for DMP/TMP, it is 0.48 (0.45 in the experiment). For toluene, the literature value is 0.26, while the experiment shows 0.22. Thus all measured values are close to the literature values; again this confirms a low OH concentration during the experiment.

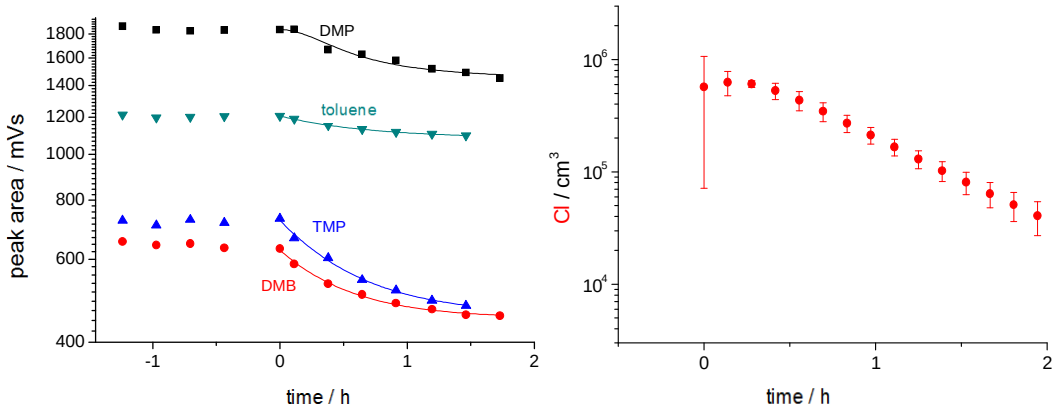

Figure 24: The low depletion of toluene above a FeCl3/NaCl salts ample with added oxalic acid (left) and the calculated Cl concentrations

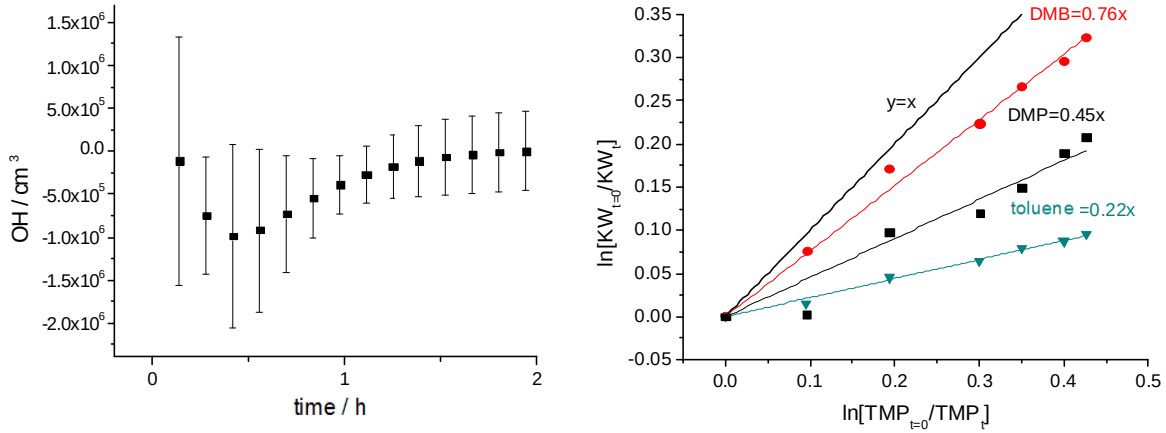

Figure 25: The calculated OH concentration oscillates around zero (left). The slopes of the lines shown right represent the ratio of the rate constants towards Cl shown in Table 1 and indicate the absence of OH

Table 18: Fitted functions represent the measurement data from Figure 24

Hydrocarbon	Fitting function/mVs
2,2-Dimethylpropane (DMP)	$1416 + 473e^{-t/2781s}$
2,2-Dimethylbutane (DMB)	$450 + 176e^{-t/1868s}$
2,2,4-Trimethylpentane (TMP)	$458 + 266e^{-t/2066s}$
Toluene	$1083 + 124e^{-t/2430s}$

3.12 $FeCl_3$, Na_2SO_4 and oxalic acid

The salt sample in this experiment contained 91 g NaCl, 2 g $FeCl_3$, 2 g oxalic acid and 5 g Na_2SO_4. The color of the crystallized salt was still orange, but much paler than the salt sample of 2.6. In light conditions a depletion of toluene was observed during the first two hours (Figure 26, left). The loss of alkanes was low, but steadily resulting from a Cl concentration just above the detection limit (Figure 26, right).

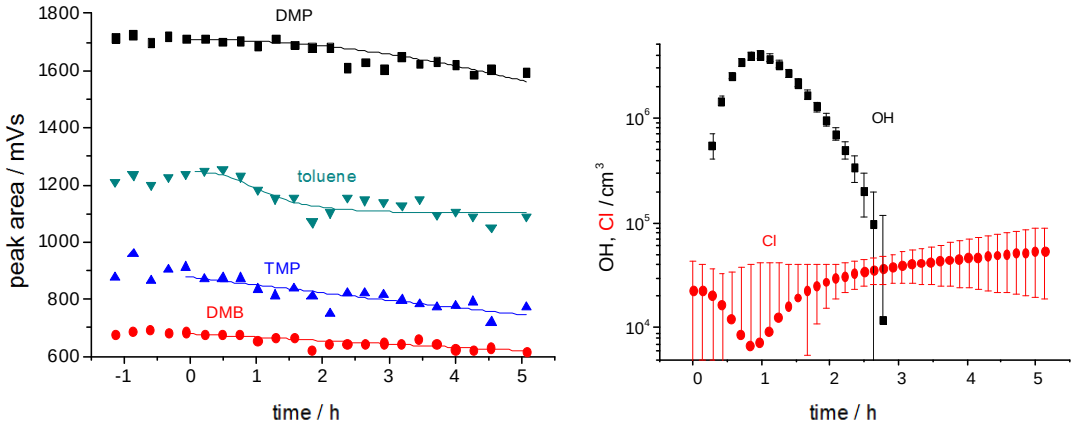

Figure 26: HC depletion over a NaCl/$FeCl_3$/$H_2C_2O_4$/ Na_2SO_4 sample (left). The chloride activation was inhibited due the addition sodium sulfate (right).

Table 19: Fitting functions to represent the HC data measured in experiment 3.12

Hydrocarbon species	Fitting function/mVs
2,2-Dimethylpropane (DMP)	$1710 - 5 \times 10^{-5} t/s - 4.5 \times 10^{-7} t^2/s^2$
2,2-Dimethylbutane (DMB)	$677e^{-t/211930s}$
2,2,4-Trimethylpentane (TMP)	$869e^{-t/122400s}$
Toluene	$1100 + \frac{1245 - 1100}{1 + (\frac{t}{4082s})^{3.0705}}$

3.13 pH values and grain sizes

The pH values of the salts were measured after the illumination (Schott CG 820 pH meter equipped with pH electrode Blue Line 16 pH). The samples were weighed and dissolved in 3 ml of bi-distilled water, or suspended (NaCl/FeCl3/Catechol sample). Table 20 summarizes the results, also shows is the treatment of the samples after the recrystallization. Table 21 shows a measured a grain size distribution.

Table 20: Overview on the preparation and the pH of the samples

Sample	Experiment Nr.	Treatment	Mass for pH det/g	pH
NaCl	3.1	milled	1,96	6,79
$NaCl/MgCl_2$	3.2	milled	1,91	7,15
NaCl/NaBr	3.3	milled	1,85	5,24
NaCl/Na-Oxalate	3.4	milled	1,71	6,56
NaCl/Catechol	3.5	ground	1,84	3,69
$NaCl/FeCl_3$	3.6a-j	ground	0,86	1,91
$NaCl/FeCl_3/Na_2SO_4$	3.7	milled	1,72	1,57
$NaCl/FeCl_3/NaC_2O_4$	3.9	untreated	1,55	5,68
$NaCl/FeCl_3$/Catechol	3.10	untreated	1,8	1,33
$NaCl/FeCl_3/H_2C_2O_4$	3.11	untreated	1,94	5,09
$NaCl/FeCl_3/Na_2SO_4/H_2C_2O_4$	3.12	grind	1,8	5,2

Table 21: Grain size of sample 3.7, determined with Retsch-sieve (DIN 4188)

Grain size	**Fraction**
> 2 mm	43.5 %
> 1 mm	21.5 %
> 630 µm	11.5 %
> 200 µm	18.5 %
< 200 µm	5 %

4 Discussion

The experiments carried out above various salt mixtures show a release of chlorine to the gas phase in dependence of the $FeCl_3$ added to the sample. The concentrations of chlorine atoms were determined by the consumption of an injected mixture of hydrocarbons, which are a sink for chlorine atoms. The measured concentration of chlorine atoms is therefore dependent on the injected amount of HC according to equation 1:

$$\frac{\mathrm{d[Cl]}}{\mathrm{d}t} = \frac{\mathrm{d[Q]}}{\mathrm{d}t} - \sum_i k_i [\mathrm{HC}_i]_t \times [\mathrm{Cl}] \quad (1)$$

where Q is the source for the chlorine atoms. The sum of the products of the HC concentrations with their rate constants k_i towards reaction with Cl-atoms is called Cl-reactivity hereafter. The Cl-concentration is kept low due to the high reactivity of the HCs. Therefore, a simplified photostationary state between the source and the sinks is assumed (d [Cl] / dt = 0). At zero time the total HC concentration is known. This allows us to calculate the maximum value of Q in eq. 1 from the initial concentration of the HCs. By using actual measured, not dilution corrected HC values and neglecting their reaction products, which have a reaction rate towards Cl as well, the minimum value of Q can be calculated.

Most of the measurement results show a significant decrease of the Cl concentration after the first hour of illumination of the sample (Figure 27, left). The reason is not clear yet; possible are changes in the measurement system, such as drying out of the salt sample or an increase of the total Cl reactivity of products formed from the HCs in the mixture during consumption. Therefore Q was only integrated over the first hour of the experiments. Table 22 summarizes the calculated results on the source strength Q. Exact values for Q can be calculated by the HALOBOX model (Bleicher, 2012), which includes the HC transformation products down to CO_2 by using the Master Chemical Mechanism from the University of Leeds.

The blank experiments without an addition of $FeCl_3$ (3.1 to 3.5) reflect the typical OH values in the chamber with added HCs of (1 ... 10) × 10^6 cm^{-3}. It was attempted to keep the injection of HC in all experiments as equal as possible. OH radicals are significantly affected by ozone (and humidity) as can be seen in experiments 3.1a and 3.1b. During both runs the OH concentration is correlated with ozone. The underlying mechanism of ozone and OH production is driven by the oxidation of the injected hydrocarbons and due to NO_X impurities:

$$\mathrm{HC + OH, Cl \rightarrow RO_2 + H_2O, HCl} \quad \text{(R1)}$$

$$\mathrm{NO + RO_2 \rightarrow NO_2 + RO}$$

$$\mathrm{NO_2 + h\nu \rightarrow NO + O}$$

$$\mathrm{O + O_2 + M \rightarrow O_3 + M}$$

$$\mathrm{O_3 + h\nu \rightarrow O(^1D) + O_2}$$

$$\mathrm{O(^1D) + H_2O \rightarrow 2\ OH}$$

In cases of high initial ozone mixing ratios, as in Experiment 3.1b, an immediate increase of the OH concentration is observed. Both, ozone and NO_X affect also the concentration of chlorine atoms in the gas phase, as can be seen in 3.1b. The concentration of Cl is well above the detection limit and

has smaller error bars in comparison to 3.1a. An activation of chloride in the presence of ozone and NO_X has been already observed on sea spray aerosol (eg. Bleicher, 2012, Buxmann, 2012).

Table 22: Overview on the experiment number with the sample composition and the measured HC mixing ratios at t = 0. The maximum of the measured concentrations and Cl to Eq. 1 minmax calculated estimates of the Cl source Q. For the calculation of Q only the first hour of the experiment was used.

Exp. Nr.	Sample	Composition (g)	Dilution (l/min)	$[Cl]_{max}$ (cm^{-3})	$[HC]_0$ (ppb)	Cl-reac. (s^{-1})	Cl-source Q (cm^{-3}) Min	Max
3.1a	NaCl	100	4.8	6.4×10^{4}	37.5	114	5.4×10^{9}	7.1×10^{9}
3.1b	NaCl with O_3. NO_X	100	4.8	7.8×10^{4}	16.4	53	7.3×10^{9}	8.3×10^{9}
3.2	$NaCl/MgCl_2$	95 / 5	4.3	2.3×10^{4}	19.6	62	1.9×10^{9}	2.5×10^{9}
3.3	NaCl/NaBr	99.5 / 0.5	6.6	4.7×10^{5}	16.5	60	1.6×10^{10}	1.9×10^{10}
3.4	NaCl/Na-Oxalate	98 / 2	4.2	1.3×10^{5}	14.0	44	1.5×10^{10}	1.8×10^{10}
3.5	NaCl/Catechol	98 / 2	4.8	3.9×10^{4}	12.8	41	4.8×10^{9}	5.3×10^{9}
3.6a	$NaCl/FeCl_3$	98 / 2	4.5	4.9×10^{7}	22.8	72	3.9×10^{11}	2.8×10^{12}
3.6b	$NaCl/FeCl_3$	98 / 2	2.9	2.4×10^{6}	47.0	132	3.5×10^{11}	6.0×10^{11}
3.6c	$NaCl/FeCl_3$	99.5 / 0.5	4.6	5.4×10^{6}	83.1	284	4.4×10^{11}	5.1×10^{11}
3.6d	$NaCl/FeCl_3$	99.5 / 0.5	5.0	4.5×10^{6}	74.9	227	8.0×10^{11}	1.6×10^{12}
3.6e	$NaCl/FeCl_3$	99.5 / 0.5	5.0	8.4×10^{5}	63.4	195	1.2×10^{11}	1.6×10^{11}
3.6f	$NaCl/FeCl_3$	99.5 / 0.5	2.6	4.6×10^{4}	103.6	353	5.2×10^{10}	6.3×10^{10}
3.6g	$NaCl/FeCl_3$	99.5 / 0.5	6	3.2×10^{6}	33.9	112	1.7×10^{11}	2.0×10^{11}
3.6j	$NaCl/FeCl_3$	99.5 / 0.5	5.4	2.4×10^{5}	26.7	88	4.4×10^{10}	5.2×10^{10}
3.7	$NaCl/FeCl_3/Na_2SO_4$	93 / 5 / 2	4.8	3.1×10^{5}	21.4	71	6.0×10^{10}	6.5×10^{10}
3.8	$NaCl/FeCl_3$/NaBr	97.5 / 0.5 / 2	4.2	8.5×10^{5}	95.0	353	4.4×10^{10}	5.3×10^{10}
3.9	$NaCl/FeCl_3/NaC_2O_4$	96 / 2 / 2	6	6.9×10^{4}	115.5	235	4.3×10^{10}	4.7×10^{10}
3.10	$NaCl/FeCl_3$/Catechol	96 / 2 / 2	4.2	2.7×10^{3}	89.6	297	2.3×10^{9}	2.7×10^{9}
3.11	$NaCl/FeCl_3/H_2C_2O_4$	96 / 2 / 2	4.2	6.3×10^{5}	27.7	85	6.8×10^{10}	9.0×10^{10}
3.12	$NaCl/FeCl_3/Na_2SO_4/H_2C_2O_4$	91 / 5 / 2 / 2	6	5.5×10^{4}	28.4	90	3.5×10^{9}	3.7×10^{9}

There are several mechanisms of chloride activation: First, there is the NO_X mechanism where N_2O_5 reacts heterogeneously on the liquid surface in the dark with chloride to form $ClNO_2$ and nitrate. In light conditions $ClNO_2$ is photolyzed to chlorine atoms and NO_2:

$$NO_2 + O_3 \rightarrow NO_3 + O_2 \qquad (R2)$$
$$NO_3 + NO_2 + M \rightarrow N_2O_5 + M$$
$$N_2O_5 + Cl^- \rightarrow ClNO_2 + NO_3^-$$
$$ClNO_2 + h\nu \rightarrow Cl + NO_2$$

A further mechanism, which works by dissolved ozone in the liquid phase, is known to activate bromide (Hunt et al., 2004). It is also conceivable to activate chloride under special conditions:

$$O_3 \rightarrow O_3(aq) \qquad (R3)$$
$$O_3(aq) + Cl^- + H^+ \rightleftharpoons HOCl + O_2$$
$$HOCl + Cl- + H^+ \rightleftharpoons Cl_2(aq) + H_2O$$
$$Cl_2(aq) \rightarrow Cl_2$$

Here chloride is oxidized by ozone and subsequently converted in the presence of protons to Cl_2. Chlorine degases afterwards due to its low solubility. However, the $HOCl/Cl_2$ equilibrium starts to shift to Cl_2 below a pH value of 3 (da Rosa, 2003).

An experiment with additional hygroscopic $MgCl_2$ (3.2) had no effect on the chloride activation.

The addition of NaBr in the experiment 3.3 led to a strong activation of bromide and chloride. The activation process of bromide is similar to R3, but runs already below a pH value of 6.5. It can activate chloride if HOBr recombines with chloride to form BrCl:

$$HOBr(aq) + H^+ + Cl^- \rightarrow BrCl(aq) + H_2O \qquad (R4)$$
$$BrCl(aq) \rightarrow BrCl$$
$$BrCl + h\nu \rightarrow Br + Cl$$

Both experiments with additional bromide show initial peaks of Br and Cl, which decrease in the first hour to a plateau for two reasons: on the one hand the heating of the sample by the irradiation leads to a loss of the aqueous layers on the crystals. On the other hand, the releasing mechanism R4 depletes the protons of the sample.

The addition of sodium oxalate in experiment 3.4 increased the chlorine concentration above 10^5 cm^{-3}. It is noteworthy that the value is higher than in Experiment 3.1b where ozone and NO_2 were injected. Possible explanation is an acidification of the sample by oxalate. The blank experiment with catechol (3.5) showed almost no chlorine release.

During the subsequent main experiments with additional iron (III) chloride extreme concentrations of chlorine and OH were observed. Depending on the addition of additives, the release varied by several orders of magnitude. The highest values were observed in pure $NaCl/FeCl_3$-mixtures, reaching concentrations above 10^7 cm^{-3} for chlorine atoms and more than 10^8 cm^{-3} OH molecules. It seems unlikely that the highly reactive radicals degas directly from the aqueous phase. Imaginable is the degasing of stable intermediates such as Cl_2, which may transfer from the liquid to the gas phase and thus represent the Cl source here.

It is known that iron (III) ions in aqueous solution enter complexes with chloride and water:

$$[Fe(OH_2)_6]^{3+} \rightleftharpoons [Fe(OH_2)_5(OH)]^{2+} + H^+ \quad (R5)$$
$$[Fe(OH_2)_6]^{3+} + Cl^- \rightleftharpoons [Fe(OH_2)_5Cl]^{2+} + H_2O$$
$$[Fe(OH_2)_6]^{3+} + 2Cl^- \rightleftharpoons [Fe(OH_2)_4Cl_2]^{+} + H_2O$$

These equilibria are dependent on the pH value (Lim, 2006, Parkhurst et al, 1999). The $[Fe(OH_2)_5(OH)]^{2+}$, $[Fe(OH_2)_5Cl]^{2+}$ und $[Fe(OH_2)_4Cl_2]^{+}$ complexes absorb light in the UV-visible range from 270 to 400 nm (Weschler et al., 1986, Faust and Hoigné, 1990). This leads to photodissociation and the formation of chlorine atoms and OH radicals under sunlight (Faust and Hoigné, 1990, Baxendale and Magee, 1955):

$$[Fe(OH_2)_5(OH)]^{2+} + H_2O + h\nu \rightarrow [Fe(OH_2)_6]^{2+} + OH \quad (R6)$$
$$[Fe(OH_2)_5Cl]^{2+} + H_2O + h\nu \rightarrow [Fe(OH_2)_6]^{2+} + Cl$$
$$[Fe(OH_2)_4Cl_2]^{+} H_2O + h\nu \rightarrow [Fe(OH_2)_6]^{2+} + Cl$$

The radicals, still in the liquid phase, react with chloride to Cl_2^- and $ClOH^-$ intermediates (Nadtochenko and Kiwi, 1998b, King et al., 1993):

$$Cl + Cl^- \rightleftharpoons Cl_2^- \quad (R7)$$
$$OH + Cl^- \rightleftharpoons ClOH^-$$

A further rearrangement forms the stable product Cl_2, which degases (Nadtochenko and Kiwi, 1998b, King et al., 1993):

$$Cl_2^- + Cl_2^- \rightleftharpoons Cl_3^- + Cl^- \quad (R8)$$
$$Cl_3^- \rightleftharpoons Cl_2 + Cl^-$$

The rearrangement is only effective at pH values below 3 (eg. da Rosa, 2003).The subsequent photolysis to two chlorine radicals in the gas phase is the prestage for methane depletion

$$Cl + HC \rightarrow HCl + RO_2 \quad (R9)$$

The resulting RO_2 radicals form ozone in mechanism (R1). The acidification of the liquid phase by the HCl formed in R9 is negligible compared to the initial acidification by iron in the atmosphere. In a closed chamber, however, the salt sample is more exposed to the formed HCl than would be the case in an open atmosphere. This is shown by the pH comparison of the samples 3.6a-b to the sample 3.6c-i in Table 20: the lower pH of the latter is understandable due to the longer exposure and overall larger HC depletion. Moreover, the repeated exposure of the second sample showed that chlorine can be released many times from the sample, if the salt is moistened. In each experiment, the release slowed down during the first hour to a plateau, which is probably a result of drying out of the liquid phase. After rewetting the sample overnight subsequent experiments showed chlorine concentrations in the range 10^6 - 10^7 cm^{-3} (Figure 27, left).

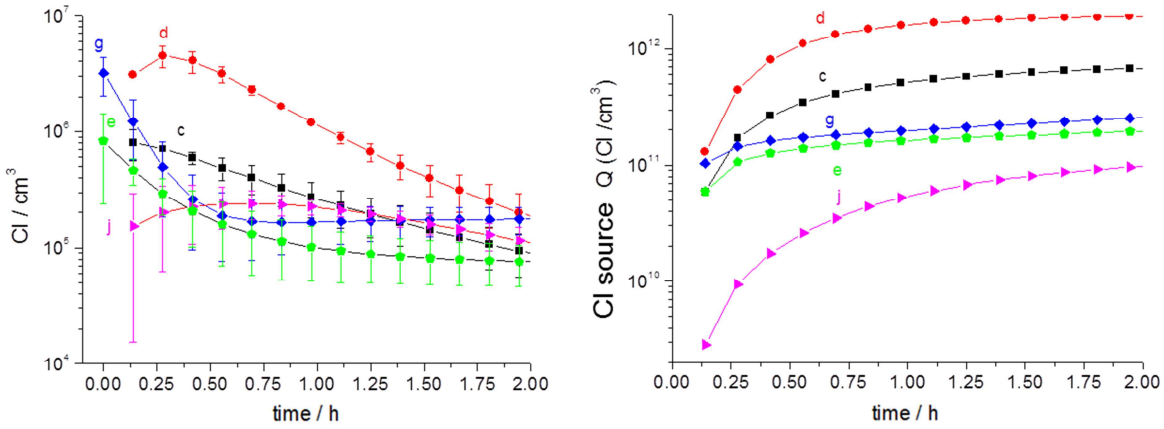

Figure 27: measured Cl concentration and the calculated Cl-source

The addition of sodium sulfate, sodium oxalate and catechol to the NaCl/$FeCl_3$ mixture hindered the chloride activation drastically. In all cases the color of the sample changed compared to the NaCl/$FeCl_3$-sample. The catechol sample was black, while the oxalate and sulfate samples were pale orange or yellow. All species, sulfate, oxalate and catechol bind via the oxygen atoms to the iron. This bonding seems to be energetically favored over chloride, so that the equilibria R5 and R6 are shifted. In the oxalate case three molecules bind twofold to the iron cation and form a $Fe[C_2O_4]^{3-}$ oxalate complex. Such double bonds are also conceivable for catechol, where both hydroxyl groups drop their proton and form an iron complex:

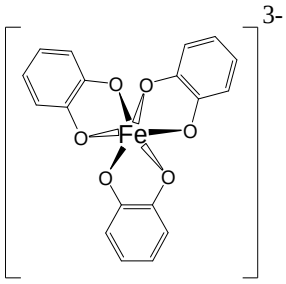

The loss of two protons per molecule explains the low pH of the catechol sample (Table 20). In experiments with bromide containing samples Br mixing ratios in the upper ppt range were measured, while the activation of the chlorine was considerably suppressed. The comparison of the bromide experiments (3.3 and 3.8) shows a difference in the behavior of both, chlorine and bromine. The initial Cl and Br concentration peaks are missing in the iron experiment entirely, instead a high nearly constant plateau of bromine atoms is observed. The release of chlorine is suppressed by bromine here, which is an indication for iron complex chemistry. While the presents of bromide leads to a recombination to BrCl in the first case (R4), in the second case the bromide ions seem to displace the chlorine in the complex bindings to iron in mechanism R5 and R6.

Overall the release of chlorine reduces the life time of methane and other hydrocarbons by reaction R8. With steady Cl concentrations of 10^6 atoms cm^{-3} the methane life time is shortened to approximately one-tenth:

$$k_{Methane,Cl} \times c_{Cl} \cong 10^{-7}\ s^{-1} \equiv 230\ d,\ (12\ h\ light\ per\ day)$$

Since OH radicals are also formed, a further shortening of the residence time is expected.

5 Conclusions and Outlook

The performed experiments yield the evidence for the activation of chloride by $FeCl_3$ in salt pans. In repeated experiments on the same sample high levels of chlorine atoms were observed in the gaseous phase. Chlorine atoms initialize the depletion of atmospheric hydrocarbons by abstraction of a H atom. The activation of chloride to chlorine can be slowed down by the addition of sodium sulfate or sodium oxalate or catechol. Catechol suppresses the activation by replacement of the chloride within the iron complex. A positive gain by catechol on the chloride activation could not be observed. Whether lower concentrations of catechol have a positive effect on the chlorine release needs to be investigated. Over ten millions chlorine atoms were measured per cm^3 above the pure mixtures of NaCl and 0.5% $FeCl_3$. Such values could reduce the methane life time to one-hundredth of its current value. However, the Cl concentration fell by two orders of magnitude after approx. one hour of illumination. A possible explanation is the drying of the aqueous phase on the salt surface due to the solar simulators irradiation. Also thinkable is change within measurement system by the increasing of the molar mixing ratio of the reactive HC due to their degradation fractioning. Specific model calculations can provide more information here.

Due to the high reactivity of Cl atoms it seems necessary to proof the possible applications of the described method in remote areas. Whether chlorinated or brominated hydrocarbons are formed has to be investigated in a further study. Also other iron species such as Fe_2O_3 must be tested for catalytic chloride activation. In particular, iron containing aerosols may have a higher specific surface than the investigated salt pans. To prove that the higher specific surface is more effective to chlorine release and thus more effective for methane depletion, follow-up studies in the environmental simulation chamber are required. In a positive case the tests will be extended to aerosols in the free troposphere, which will be limited to the air traffic at high elevations and ship traffic.

6 Appendix

6.1 Reaction rate constants of alkanes and toluene with OH and Cl

Cl atoms have fast reaction rates towards alkanes, because the abstraction reaction of H atoms is more exothermic as in the OH case. The exothermicity leads to low activation energies, the steric factor dominates here. Low selectivity of Cl reaction follows and the rate constant increases with the number of abstractable hydrogen atoms. However, aromatic CH bonds of toluene are firm and the relatively loose benzylic CH bonds are sterically less accessible. The reaction of OH with toluene dominates the addition to the aromatic ring, while for Cl atoms, the addition plays a minor role (Figure 28).

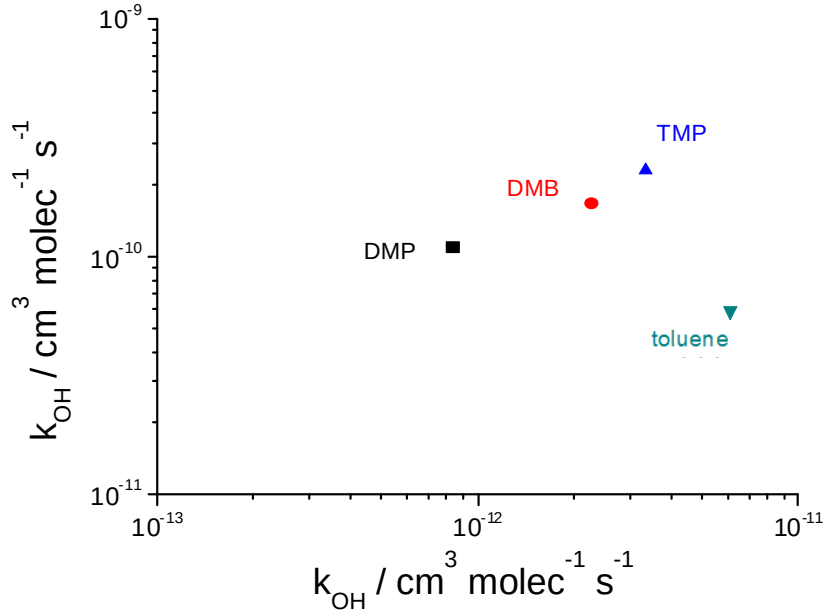

Figure 28: The ratio of reaction rates of alkanes towards OH and Cl is similar, while it is shifted to OH in the case of toluene

6.2 Conversion between Cl atom concentration to Cl mass per m^3

$$c_{Cl,OH}\left[\frac{mg}{m^3}\right] = c_{Cl,OH}\left[\frac{Atome}{cm^3}\right] \times m_{atom(Cl,OH)}[dalton] \times 1.660539 \times 10^{-24} g \times 10^{9}\left[\frac{g \rightarrow mg}{cm^3 \rightarrow m^3}\right]$$

	Atoms/cm^3	g/ m^3	mg/ m^3	ng/ m^3	Molar mass (g/mol)
Cl	10^7	5.89×10^{-10}	5.89×10^{-7}	0.59	35.5
OH	10^7	2.8×10^{-10}	2.8×10^{-7}	0.28	17

6.3a Mathematica script for OH/Cl-evaluation (Experiment 3.1b)

```
(*Temperature, T, and the activation energies units are in Kelvin, the time t is in seconds.*)

(*Zuordnung der, an die Messergebnisse angepassten, hier sigmoiden Funktionen*)
NeoP[t_]:= 552+(936-552)/(1+(t/39164)^1.1535)
DMB[t_]:=322+(437.6-322)/(1+(t/9815.8)^1.66026)
TMP[t_]:=324.9+(572-324.9)/(1+(t/12560)^1.25525)
toluol[t_]:=357.5+(714.5-357.5)/(1+(t/11515)^0.75906)

(*Aufstellung der Differentialgleichungen mit Gewichtung durch die Geschwindigkeitskonstanten. Da die
angepassten Funktionen differenzierbar sind, ist dies im strengeren Sinn ein überbestimmtes lineares
Gleichungssystem mit zwei Unbekannten.*)
k1:=NeoP'[τ]==-1.65 10^-12 (T/298)^2×exp(-1720/T)× NeoP[τ] OH - 1.11 10^-10 NeoP [τ]Cl
k2:=DMB'[τ]==-3.37 10^-11 ×exp(-809/T) ×DMB[τ] OH- 1.68 10^-10 DMB[τ] Cl
k3:=TMP'[τ]==-2.09 10^-12  ×exp(-1160/T) ×TMP [τ]OH-2.26 10^-10 TMP[τ]Cl
k4:=toluol'[τ]==-2.09 10^-12  ×exp(322/T) ×toluol[τ] OH   - 5.90 10^-11 toluol[τ] Cl

(*Header*)
array={"Zeit\toh12\toh13\toh14\toh23\toh24\toh34\tMittelOH\tstdOH\tcl12\tcl13\tcl14\tcl23\tcl24\tcl
34\tMittelCl\tstdCl"};
T=298; (*Temperatur*)
i=0;
While[i<38, (*Zeitschritte*)
 τ=i 500; (*Zeitauflösung*)
 e12:={Cl,OH}/.Solve[{k1,k2},{Cl,OH}]; (*Paarweise Lösung des lin. Gleichungssystems*)
 e13:={Cl,OH}/.Solve[{k1,k3},{Cl,OH}]; (*und Zuordnung zu den Vektoren e*)
 e14:={Cl,OH}/.Solve[{k1,k4},{Cl,OH}];
 e23:={Cl,OH}/.Solve[{k2,k3},{Cl,OH}];
 e24:={Cl,OH}/.Solve[{k2,k4},{Cl,OH}];
 e34:={Cl,OH}/.Solve[{k3,k4},{Cl,OH}];

 oh12=e12[[1,2]]; cl12=e12[[1,1]]; (*Auflösung der Vektoren in zwei Skalare*)
 oh13=e13[[1,2]]; cl13=e13[[1,1]];
 oh14=e14[[1,2]]; cl14=e14[[1,1]];
 oh23=e23[[1,2]]; cl23=e23[[1,1]];
 oh24=e24[[1,2]]; cl24=e24[[1,1]];
 oh34=e34[[1,2]]; cl34=e34[[1,1]];

(*Berechnung des Mittelwerts und der Standardabweichung, hier nur unter Berücksichtigung der Alkan-
Toluol Lösungen*)
Mittel=(e24+e14+e34)/3;
std=\[Sqrt](1/2((e24-Mittel)^2+(e14-Mittel)^2+(e34-Mittel)^2));

(*Ausgabe aller Ergebnisse*)
```

```
array=Append[array,{ τ,oh12,oh13,oh14,oh23,oh24,oh34,Mittel[[1,2]],std[[1,2]],
cl12,cl13,cl14,cl23,cl24,cl34,Mittel[[1,1]],std[[1,1]]}];
 i++]
Export["C:\users\cer\desktop\OHCl.dat",array];
```

6.3b Mathematica Script zur OH/Cl/Br-Auswertung (Exp. 3.8)

```
NeoP[t_] := 2108×exp(-t/110992)
DMB[t_] := 4206×exp(-t/68077)
TMP[t_] :=  528.3 + (6.64564 10^6 - 528.3)/(1 + exp((t + 61007.46)/8078.15))
toluol[t_] :=  60.49 + (2.6118 10^6 - 450.11)/(1 + exp((t + 31237.9)/5213.6))

k1:=NeoP'[τ]==-1.65 10^-12 (T/298)^2×exp(-1720/T)× NeoP[τ] OH - 1.11 10^-10 NeoP [τ]Cl
k2:=DMB'[τ]==-3.37 10^-11 ×exp(-809/T)DMB[τ] OH- 1.68 10^-10 DMB[τ] Cl
k3:=TMP'[τ]==-2.09 10^-12  ×exp(-1160/T)TMP [τ]OH-2.26 10^-10 TMP[τ]Cl -6.8 10^-15 TMP[τ] Br
k4:=toluol'[τ]==-2.09 10^-12  ×exp(322/T)toluol[τ] OH   - 5.90 10^-11 toluol[τ] Cl-1.3 10^-14 toluol[τ] Br

array={"Zeit\toh123\toh134\toh234\tMittelOH\tstdOH\tcl123\tcl134\tcl234\tMittelcl\tstdcl\tbr123\tbr
134\tbr234\tMittelbr\tstdbr"};
T=298;
i=0;
While[i<30,
 τ=i 500;
 e123:={Cl,OH,Br}/.Solve[{k1,k2,k3},{Cl,OH,Br}];
 e134:={Cl,OH,Br}/.Solve[{k1,k3,k4},{Cl,OH,Br}];
 e234:={Cl,OH,Br}/.Solve[{k2,k3,k4},{Cl,OH,Br}];

 oh123=e123[[1,2]];
 oh134=e134[[1,2]];
 oh234=e234[[1,2]];

 cl123=e123[[1,1]];
 cl134=e134[[1,1]];
 cl234=e234[[1,1]];

 br123=e123[[1,3]];
 br134=e134[[1,3]];
 br234=e234[[1,3]];

 Mittel=(e123+e134)/2;

 std=\[Sqrt](1/1(((e123-Mittel)^2+(e134-Mittel)^2)));

 array=Append[array,{,oh123,oh134,oh234, Mittel[[1,2]],std[[1,2]],
cl123,cl134,cl234,Mittel[[1,1]],std[[1,1]],br123,br134,br234,Mittel[[1,3]],std[[1,3]]}];
 i++]
Export["C:\Users\cer\Desktop\OHCl.dat",array];
```

Literature

Adhikamsetty, R. K. and S. B. Jonnalagadda (2009), Kinetics and mechanism of Prussian blue formation, *Bull. Chem. Soc. Ethiop.,* 23(1), 47–54.

Arakaki, T., M. Shibata, T. Miyake, T. Hirakawa, H. Sakugawa (2004), Enhanced formation of formate by freezing in solutions of hydrated formaldehyde-metal-hydrogen peroxide, *Geochem J*(38), 383–388.

Baker, A. K., A. Rauthe-Schöch, T. J. Schuck, C. Am Brenninkmeijer, P. F. J. van Velthoven, A. Wisher, D. E. Oram (2011), Investigation of chlorine radical chemistry in the Eyjafjallajökull volcanic plume using observed depletions in non-methane hydrocarbons, *Geophys. Res. Lett.,* 38(13), L13801.

Balzer, N. (2012), Kinetische Untersuchungen der Halogen-Aktivierung einer simulierten Salzpfanne in einer Smogkammer, *Unveröffentlichtes Manuskript der an der Fakultät für Biologie, Chemie und Geowissenschaften der Universität Bayreuth eingereichten Dissertation*.

Barcellos da Rosa, M., P. Barzaghi, A. Donati, C. George, H. Herrmann, W.-U. Palm and C. Zetzsch IV-3. Elementary reactions in the aqueous phase 3.4 Halogen containing radical kinetics and halogen activation from aqueous particles; *C. George & H. Herrmann: IV. Multiphase chemistry of clouds and aerosols: Im pact on air quality and the ozone balance*; Internet page: imk-aida.fzk.de/CMD/final_report/IV_all.pdf

Barcellos da Rosa M. (2003): Untersuchungen heterogener troposphärenrelevanter Reaktionen von Schwefel- und Halogenverbindungen, *Dissertation Fachbereich Chemie der Universität Hannover.*

Barnes, I., V. Bastian, K. H. Becker, R. Overath, Z. Tong (1989), Rate constants for the reactions of Br atoms with a series of alkanes, alkenes, and alkynes in the presence of O2, *Int. J. Chem. Kinet.,* 21(7), 499–517.

Batel, F., M.E. Böttcher, K. Bosselmann, H.-J. Brumsack, B.B. Jörgensen (2005): Biogeochemische Stoffumsätze im S-Mn-Fe-Kreislauf eines tidalen Oberflächensediments der südlichen Nordsee: Eine experimentelle Studie, *Sediment 2003 [Hrsg.: Alfred-Wegener-Stiftung. Verantw. Achim Wegemann]*, Bonn 2003; S. 83 ISSN 0946-8978

Baxendale, J. H. and J. Magee (1955), The photochemical oxidation of benzene in aqueous solution by ferric ion, *Transactions of the Faraday Society,* 51, 205–213.

Binenga, Y. (2006): Chemical Analysis of the Assale (Ethiopia) rock salt deposit; *Bull. Chem. Soc. Ethiop.*, 20(2), pp. 319-324

Bleicher, S.: Zur Halogenaktivierung im Aerosol und in Salzpfannen, Unveröffentlichtes Manuskript der an der Fakultät für Biologie, Chemie und Geowissenschaften der Universität Bayreuth eingereichten Dissertation, 2012.

Bobrowski, N., R. von Glasow, A. Aiuppa, S. Inguaggiato, I. Louban, O. W. Ibrahim, U. Platt (2007), Reactive halogen chemistry in volcanic plumes, *J. Geophys. Res.,* 112(D6), 2156–2202, doi:10.1029/2006JD007206.

Borges, F., C. Guimarães, J. L. Lima, I. Pinto, S. Reis (2005), Potentiometric studies on the complexation of copper (II) by phenolic acids as discrete ligand models of humic substances, *Talanta,* 66(3), 670–673.

Bryukov, M. G., I. R. Slagle, V. D. Knyazev (2002), Kinetics of reactions of Cl atoms with methane and chlorinated methanes, *J. Phys. Chem. A,* 106(44), 10532–10542.

Buxmann, J., N. Balzer, S. Bleicher, U. Platt, C. Zetzsch (2012), Observations of bromine explosions in smog chamber experiments above a model salt pan, *Int. J. Chem. Kinet.,* 44(5), 312–326, doi:10.1002/kin.20714.

Buxmann, J., S. Bleicher, U. Platt, C. Zetzsch:„Chlorine Explosion“ an autocatalytic *release from sea salt aerosols, Poster bei der Solas Open Science Conference 2012*

Buxmann, J., R. Holla, U. Platt, K. Kotte, N. Balzer, S. Bleicher, C. Zetzsch: Bromine explosions in smog chamber experiments above a model salt pan, *webpresentatio,* web.mit.edu/icck/presentations/ICCK219oral%20.pdf 2012

Buxmann, J.: “Bromine and chlorine explosion” in a simulated atmosphere, Dissertation, Fakultät für Physik der Universität Heidelberg, 2012

Chiron, S., C. Minero, D. Vione (2007), Photodegradation of xenobiotic compounds relevant to estuarine waters, *Annali di chimica,* 97(3-4), 135–139.

Claeys, M., R. Vermeylen, F. Yasmeen, Y. Gómez-González, X. Chi, W. Maenhaut, T. Mészáros, I. Salma (2012), Chemical characterisation of humic-like substances from urban, rural and tropical biomass burning environments using liquid chromatography with UV/vis photodiode array detection and electrospray ionisation mass spectrometry, *Environ. Chem.,* 9(3), 273–284, doi:10.1071/EN11163.

Coates, J.D.: Anaerobic microbial metabolism with humic substances*: Symp. On refractory organic substances in the environment – ROSE 06.-08.10.1997 am Engler-Bunte- Institut der Univ. Karlsruhe*

Deguillaume, L., K. V. Desboeufs, M. Leriche, Y. Long, N. Chaumerliac (2010), Effect of iron dissolution on cloud chemistry: from laboratory measurements to model results, Atmos, *Pollut. Res,* 1(4), 220–228.

Duggen, S., P. Croot, U. Schacht, L. Hoffmann (2007), Subduction zone volcanic ash can fertilize the surface ocean and stimulate phytoplankton growth: Evidence from biogeochemical experiments and satellite data, *Geophys. Res. Lett.,* 34(1), doi:10.1029/2006GL027522.

Eder, J. M. (1880), Über die Zersetzung des Eisenchlorides und einiger organischer Ferridsalze im Lichte, *Monatshefte für Chemie/Chemical Monthly,* 1(1), 755–762.

Eder, J.M.: Neue Untersuchungen über lichtempfindliche Salze*, Photographische Correspondenz*, **1880,** XVII, p. 219 (Zitat entnommen aus Pizzighelli, J. & Baron Hübl, A. „Die Platinotypie“, 1883, Verlag der Photographischen Correspondenz)

Faust, B. C. and J. Hoigné (1990), Photolysis of Fe (III)-hydroxy complexes as sources of OH radicals in clouds, fog and rain, *Atmospheric Environment. Part A. General Topics,* 24(1), 79–89.

Fu, H., D. M. Cwiertny, G. R. Carmichael, M. M. Scherer, V. H. Grassian (2010), Photoreductive dissolution of Fe-containing mineral dust particles in acidic media, *J. Geophys. Res.,* 115(D11), D11304, doi:10.1029/2009JD012702.

Gauci, V., S. Blake, D. S. Stevenson, E. J. Highwood (2008), Halving of the northern wetland CH 4 source by a large Icelandic volcanic eruption, *J. Geophys. Res.,* 113, doi:10.1029/2007JG000499.

Glasow, R. von, N. Bobrowski, C. Kern (2009), The effects of volcanic eruptions on atmospheric chemistry, *Chem. Geol.,* 263(1-4), 131–142, doi:10.1016/j.chemgeo.2008.08.020.

Grannas, A. M., A. R. Bausch, K. M. Mahanna (2007), Enhanced Aqueous Photochemical Reaction Rates after Freezing, *J. Phys. Chem. A,* 111(43), 11043–11049, doi:10.1021/jp073802q.

Herrmann H., B. Ervens, J. Hesper, F. Wicktor (2007)**:** Tropospheric aqueous phase chemistry laboratory and modeling studies, *Internet-Publication*, www.cert.ucr.edu/~carter/epacham/herrmann.pdf

Hunt, S. W., M. Roeselova, W. Wang, L. M. Wingen, E. M. Knipping, D. J. Tobias, D. Dabdub, B. J. Finlayson-Pitts (2004), Formation of molecular bromine from the reaction of ozone with deliquesced NaBr aerosol: evidence for interface chemistry, *J. Phys. Chem. A,* 108(52), 11559–11572.

Ito, A. (2013), Global modeling study of potentially bioavailable iron input from shipboard aerosol sources to the ocean, *Global biogeochem. cycle,* 27(1), 1–10, doi:10.1029/2012GB004378.

IPCC Fourth Assessment Report: Climate Change (2007). Working Group I: The Physical Science Basis. Atmospheric Methane. Abschnitt 2.3.2

Johnson, M. and N. Meskhidze (2011): Updated dust-irondissolution mechanism in GEOSChem: Effects of organic acids photolysis, cloud cycling, and dust mineralogy, *5th North Carolina State University GEOS-Chem Users' Meeting* May 2, 2011

Khanra, S., C. Minero, V. Maurino, E. Pelizzetti, B. Dutta, D. Vione (2008), Phenol transformation induced by UVA photolysis of the complex FeCl2+, *Environ Chem Lett,* 6(1), 29-34, doi:10.1007/s10311-007-0108-z.

Kim, E., Y. Liu, C. J. Baker, R. Owens, S. Xiao, W. E. Bentley, G. F. Payne (2011), Redox-Cycling and H 2 O 2 Generation by Fabricated Catecholic Films in the Absence of Enzymes, *Biomacromolecules,* 12(4), 880–888, doi:10.1021/bm101499a.

Kim, K., W. Choi, M. R. Hoffmann, H.-I. Yoon, B.-K. Park (2010), Photoreductive Dissolution of Iron Oxides Trapped in Ice and Its Environmental Implications, *Environ. Sci. Technol.,* 44(11), 4142–4148, doi:10.1021/es9037808.

Kirnbauer, T. (2008): Hydrothermale Bildungen des Thermalwassersystems von Bad Nauheim (Wetterau) und dessen Alter*; Jber. Wetterau. Ges. ges. Naturkunde*, 18(2), 39-96

Kotte, K. & Schöler, H.F. (2010): Öde Wüsten, versalzene Seen – wie der Klimawandel das Gesicht der Erde verändert*, Internet-Publikation der Universität Heidelberg*, www.uni-heidelberg.de/presse/ruca 2010-2/4geo.html

Krause, T., S. Studenroth, S.G. Huber, H.F. Schöler : The abiotic degradation of soil organic matter; Co-Evolution of soils and organic substances: Links between solid forming processes and the stabilization of organic substances, 2nd – 4th March 2011, Landau/Pfalz*, Conference guide and abstracts p. 42*

Krause, T.: unveröffentlichte Daten**,** 2013

Langmann, B., K. Zakšek, M. Hort, S. Duggen (2010), Volcanic ash as fertiliser for the surface ocean, *Atmos. Chem. Phys,* 10(8), 3891–3899.

Levine, J. G., E. W. Wolff, A. E. Jones, L. C. Sime (2011), The role of atomic chlorine in glacial-interglacial changes in the carbon-13 content of atmospheric methane, *Geophys. Res. Lett.,* 38(4), doi:10.1029/2010GL046122.

Levine, J.G., E. W. Wolff, A. E. Jones , M.A. Hutterli, L.C. Sime, O. Wild, P.J. Valdes, P.O. Hopcroft, A.T. Archibald, G.D. Carver, N.J. Warwick, J.A. Pyle: The ice-core record of atmospheric methane: Composition-climate interactions on timescales of tens of thousands of years*;* Internet-EGU-Publication **2012**: presentations.copernicus.org/EGU2012-9540_presentation.pdf

Lim, M., K. Chiang, R. Amal (2006), Photochemical synthesis of chlorine gas from iron(III) and chloride solution, *J. Photochem. Photobiol. A-Chem.,* 183(1-2), 126–132, doi:10.1016/j.jphotochem.2006.03.005.

Lindenthal, A., B. Langmann, J. Paetsch, I. Lorkowski, M. Hort (2012), The ocean response to volcanic iron fertilisation after the eruption of Kasatochi volcano: a regional scale biogeochemical ocean model study, *Biogeosciences Discuss.,* 9(7), 9233–9257, doi:10.5194/bgd-9-9233-2012.

Lovley, D. R., J. D. Coates, E. L. Blunt-Harris, E. J. P. Phillips, J. C. Woodward (1996), Humic substances as electron acceptors for microbial respiration, *Nature,* 382(6590), 445–448.

Machulek, A., C. Vautier-Giongo, J. E. F. Moraes, C. A. O. Nascimento, F. H. Quina (2006), Laser Flash Photolysis Study of the Photocatalytic Step of the Photo-Fenton Reaction in Saline Solution†, *Photochem. photobiol.,* 82(1), 208–212.

Madronich, S., G. J. Velders, J. Daniel, M. Lal, A. McCulloch, H. Slaper (1998), Halocarbon scenarios for the future ozone layer and related consequences, *Scientific assessment of ozone depletion,* 998, 11–1.

Madu, A.N., Njoku, P.C., Iwuoha, G.A. (2011), Extent of heavy metals in oil samples in Escravous, Abiteye and Malu platforms in Delta State Nigeria; Learning Publics Journal of Agricultural and Environmental Studies, 2(2), pp. 41-44

Mercê, A. L. R., C. Greboge, G. Mendes, A. S. Mangrich (2005), Molybdenum (VI) binded to humic and nitrohumic acid models in aqueous solutions: phthalic, 3-and 4-nitrophthalic acids, catechol and 4-nitrocathecol, part 1, *JBCS,* 16(1), 37–45.

Meyer-Oeste, F.D.: Mit Vitalelementen und/oder Schutzstoffen angereicherte troposphärische Raumelemente; PCT-Patentanmeldung Int. Veröffentlichungs-Nr. WO 03/013698 A2, Int. Veröffentlichungsdatum: 20.02.2003

Meyer-Oeste, F.D.: Chloremittierende Schicht; Deutsche Patentanmeldung Aktenzeichen 102012017734.8 Priorität der Anmeldung vom 31.08.2012 Voraussichtliches Veröffentlichungsjahr: Februar 2014

Miura, Y. H., I. Tomita, T. Watanabe, T. Hirayama, S. Fukui (1998), Active oxygens generation by flavonoids, *Biol Pharm Bull,* 21(2), 93-96.

Moonshine, M., Y. Rudich, S. Katsman, E. R. Graber (2008), Atmospheric HULIS enhance pollutant degradation by promoting the dark Fenton reaction, *Geophys. Res. Lett.,* 35(20), doi:10.1029/2008GL035285.

Myriokefalitakis, S., K. Tsigaridis, N. Mihalopoulos, J. Sciare, A. Nenes, K. Kawamura, A. Segers, M. Kanakidou (2011), In-cloud oxalate formation in the global troposphere: a 3-D modeling study, *Atmos. Chem. Phys.,* 11(12), 5761–5782, doi:10.5194/acp-11-5761-2011.

Nadtochenko, V. and J. Kiwi (1998), Primary photochemical reactions in the photo-Fenton system with ferric chloride. 1. A case study of xylidine oxidation as a model compound, *Environ. Sci. Technol.,* 32(21), 3273–3281.

Nadtochenko, V. A. and J. Kiwi (1998), Mechanism of formation of phenoxyl radicals during the photo-oxidation of phenol in the presence of FeIII, *J. Chem. Soc., Perkin Trans. 2*(6), 1303–1306, doi:10.1039/a802022a.

Nadtochenko, V. A. and J. Kiwi (1998), Photolysis of FeOH2+ and FeCl2+ in aqueous solution. Photodissociation kinetics and quantum yields, *Inorg. Chem.,* 37(20), 5233–5238.

Oeste, F.D.: Climate cooling by interaction of natural (A) or artificial (B) loess dust with tropospheric methane, *Poster presented at the GeoLeipzig 2004, joint conference of the DGG and GGW*, Leipzig

Oeste, F.D. and E. Ries: CO2 and CH4 CCS by iron salt aerosol (ISA): Enduring carbon burial within the oceanic sediment by coal power flue gas, traffic systems and "cloud whitening*", Poster presented at 2nd*

International Conference on Energy process Engineering – Efficient Carbon Capture for Coal Power Plants (ICEPE 2011) June 20-22, **2011** in Frankfurt/Main

Oeste, F.D.: Verfahren zur Abkühlung der Troposphäre; PCT-Patentanmeldung Int. Veröffentlichungs-Nr. WO 2010/075856 A2, Int. Veröffentlichungsdatum: 08.07.2010

Parkhurst, D.L. and C.A.J. Appelo (1999): User's Guide to PHREEQC (Version 2) – A Computer Program For Speciation, Batch-Reaction, One-Dimensional Transport, And Inverse Geochemical Calculations, *Water Resources Investigations Report 99-4259, U.S. Geological Survey Central Region Research*, Denver

Pöhler, D., L. Vogel, U. Friess, U. Platt (2010), From the Cover: Atmospheric Chemistry Special Feature: Observation of halogen species in the Amundsen Gulf, Arctic, by active long-path differential optical absorption spectroscopy, *PNAS,* 107(15), 6582–6587, doi:10.1073/pnas.0912231107.

Shi, Z., S. Bonneville, M. D. Krom, K. S. Carslaw, T. D. Jickells, A. R. Baker, L. G. Benning (2011), Iron dissolution kinetics of mineral dust at low pH during simulated atmospheric processing, *Atmos. Chem. Phys.,* 11(3), 995–1007, doi:10.5194/acp-11-995-2011.

Siekmann, F.: Freisetzung von photolabilen und reaktiven Halogenverbindungen aus salzhaltigen Aerosolen unter simulierten troposphärischen Reinluftbedingungen in einer Aerosol-Smogkammer*, Dissertation, Fakultät für Biologie, Chemie und Geowissenschaften der Universität Bayreuth*, 2008.

Southworth, B. A. and B. M. Voelker (2003), Hydroxyl Radical Production via the Photo-Fenton Reaction in the Presence of Fulvic Acid, *Environ. Sci. Technol.,* 37(6), 1130–1136, doi:10.1021/es020757l.

Spolaor, A., P. Vallelonga, G. Cozzi, J. Gabrieli, C. Varin, N. Kehrwald, P. Zennaro, C. Boutron, C. Barbante (2013), Iron speciation in aerosol dust influences iron bioavailability over glacial-interglacial timescales, *Geophys. Res. Lett.,* 40(8), 1618–1623, doi:10.1002/grl.50296.

Spolaor, A., P. Vallelonga, J. Gabrieli, M. Roman, C. Barbante (2013), Continuous flow analysis method for determination of soluble iron and aluminium in ice cores, *Anal Bioanal Chem,* 405(2-3), 767-774, doi:10.1007/s00216-012-6166-5.

Spolaor, A., P. Vallelonga, J. Gabrieli, G. Cozzi, C. Boutron, C. Barbante (2012), Determination of Fe2+ and Fe3+ species by FIA-CRC-ICP-MS in Antarctic ice samples, *J. Anal. Atom. Spectrom.,* 27(2), 310–317.

Stewart, R. (2004), The annual cycle of hydrogen peroxide: an indicator of chemical instability?, *Atmos. Chem. Phys.*(4), 933–946.

Titler, R.V. and P. Kerry (2011): Chemical analysis of major constituents and trace contaminants of rock salt; *Publikation des Pennsylvania Department of Environmental Protection Bureau of Water Standards and Facility Regulation*

Tobo, Y., D. Zhang, A. Matsuki, Y. Iwasaka (2010), Asian dust particles converted into aqueous droplets under remote marine atmospheric conditions, *Proceedings of the National Academy of Sciences,* 107(42), 17905–17910, doi:10.1073/pnas.1008235107.

Trochkine, D., Y. Iwasaka, A. Matsuki, M. Yamada, Y.-S. Kim, D. Zhang, G.-Y. Shi, Z. Shen, G. Li (2003), Comparison of the Chemical Composition of Mineral Particles Collected in Dunhuang, China and those Collected in the Free Troposphere over Japan: Possible Chemical Modification during Long-Range Transport, *Water, Air, and Soil Pollution: Focus 3,* 2003, 161–172.

Unbekannter Autor: Celtic sea salts analysis; Internet-Seite www.curzio.com/N/Celtic_Sea_Salt1.htm

Unbekannter Autor: Celtic sea salt analysis; dowsers.com/Celtic%20Sea%20Salt%20Analysis.pdf

ur Rahman, A., A. Islam, M. A. Farrukh (2010), Preparation of Analytical Grade Sodium Chloride from Khewra Rock Salt, *World Applied Sciences Journal,* 9(11), 1223–1227.

van der Pluijm, B.A. and L.T. Sefcik: Inquiries in global change. Unit 8a. Analysis of Vostok ice core data; 14.11.2007, http://www.globalchange.umich.edu/globalchange1/current/labsLab9/Vostok.htm

Vione, D., V. Maurino, C. Minero, P. Calza, E. Pelizzetti (2005), Phenol Chlorination and Photochlorination in the Presence of Chloride Ions in Homogeneous Aqueous Solution, *Environ. Sci. Technol.,* 39(13), 5066–5075, doi:10.1021/es0480567.

Vione, D., V. Maurino, C. Minero, E. Pelizzetti, M. A. J. Harrison, R.-I. Olariu, C. Arsene (2006), Photochemical reactions in the tropospheric aqueous phase and on particulate matter, *Chem. Soc. Rev., doi:*10.1039/b510796m.

von Glasow, R.; Bobrowski, N.; Kern, C. (2009): The effects of volcanic eruptions on atmospheric chemistry. In: *Chemical Geology* 263 (1-4), S. 131–142.

Weller, C. & Herrmann, H.: Photolysis of iron(III)carboxylate complexes in aqueous Atmospheric particles, *Poster presented at the EGU 2009 in Vienna*

Weschler, C. J., M. L. Mandich, T. E. Graedel (1986), Speciation, photosensitivity, and reactions of transition metal ions in atmospheric droplets, *J. Geophys. Res.,* 91(D4), 5189–5204.

Whitney King, D., R. A. Aldrich, S. E. Charnecki (1993), Photochemical redox cycling of iron in NaCl solutions, *Marine chemistry,* 44(2), 105–120.

Zetzsch, C. and W. Behnke (1992), Heterogeneous photochemical sources of atomic Cl in the troposphere, *Berichte der Bunsengesellschaft für physikalische Chemie,* 96(3), 488–493.

Zhang, D. and Y. Iwasaka (2001), Chlorine deposition on dust particles in marine atmosphere, *Geophys. Res. Lett.,* 28(18), 3613–3616.

Zhu, X., J. M. Prospero, D. L. Savoie, F. J. Millero, R. G. Zika, E. S. Saltzman (1993), Photoreduction of iron (III) in marine mineral aerosol solutions, *J. Geophys. Res.,* 98(D5), 9039–9046.

Zhuang, G., Z. Yi, R. A. Duce, P. R. Brown (1992), Chemistry of iron in marine aerosols, *Global biogeochem. cycle,* 6(2), 161–173.